Geosci. Model Dev. Discuss., doi:10.5194/gmd-2017-75, 2017
Manuscript under review for journal Geosci. Model Dev.
Discussion started: 5 May 2017

Geoscientific Model Development Discussions

Description and Validation of the Simple, Efficient, Dynamic, Global, Ecological Simulator (SEDGES v.1.0)

Pablo Paiewonsky[1] and Oliver Elison Timm[1]

[1]Department of Atmospheric and Environmental Sciences, State University of New York at Albany, 1400 Washington Ave., Albany, NY 12222

Correspondence to: Pablo Paiewonsky (ppaiewonsky@albany.edu)

Abstract. In this paper, we present a simple vegetation model whose primary intended use is auxiliary to the land-atmosphere coupling scheme of a climate model, particularly one of intermediate complexity. The model formulations and their derivations are presented here, in detail. The model includes some realistic and useful features for its level of complexity, including a photosynthetic dependency on light, full coupling of photosynthesis and transpiration through an interactive canopy resistance, and a soil organic carbon dependence for bare soil albedo. We evaluate the model's performance by running it using a simple land surface scheme that is driven by reanalysis data. The evaluation against observational data includes net primary productivity, leaf area index, surface albedo, and diagnosed variables relevant for the closure of the hydrological cycle. In this set up, we find that the model gives an adequate to good simulation of basic large-scale ecological and hydrological variables. Of the variables analyzed in this paper, gross primary productivity is particularly well simulated. The results also reveal the current limitations of the model. The most significant deficiency is the excessive simulation of evapotranspiration in mid- to high northern latitudes during their winter to spring transition. The model has relative advantage in situations that require some combination of computational efficiency, model transparency and tractability, and the simulation of the large scale vegetation and land surface characteristics under non-present day conditions.

1 Introduction

Simulation of the land surface is a critical component of models of the Earth climate system. In such models, heat, energy, and moisture transfer between the land and atmosphere or ocean are calculated with information from the hydrological and vegetation components of these models. SEDGES simulates the gross properties of vegetation and large scale land surface characteristics, in a way as to be used by a land surface scheme in a climate or Earth system model. Models of similar complexity as SEDGES exist that simulate the vegetative if not also the hydrological and energy-transferring aspects of the land surface: VECODE (Brovkin et al., 1997, 2002) and ENTS (Williamson et al., 2006). The purpose of these kinds of models is to efficiently and reasonably simulate dynamic land surface characteristics and provide these to the atmospheric components of Earth system models of intermediate complexity. In such a framework, the need for sophisticated simulations of the land surface is obviated by the simplifications present in the other model components, by a desire to more easily understand the processes underlying experimental results, and by the computational burden that goes along with the increased complexity.

Geosci. Model Dev. Discuss., doi:10.5194/gmd-2017-75, 2017
Manuscript under review for journal Geosci. Model Dev.
Discussion started: 5 May 2017

Geoscientific Model Development Discussions

SEDGES is based on the original SimBA model (Kleidon, 2006b), which was coupled to the Planet Simulator (PlaSim) general circulation model (GCM) (Lunkeit et al., 2007) and even more strongly based on a later version of SimBA (Lunkeit et al., 2011), also coupled to PlaSim. Neither version of SimBA has been well-validated, although the earlier version has been used in a number of studies (e.g., Kleidon, 2006a, b; Dekker et al., 2010; Bowring et al., 2014). The SimBA model is based on a light and water-use-efficiency model for crops (Monteith et al., 1989) that was later adapted and expanded to forest canopies (Dewar, 1997). SEDGES builds upon SimBA by improving most of its parameterizations, incorporating the effect of aerodynamic conductance on CO_2 uptake, and including plant regulation of canopy conductance under changing light and moisture conditions. This paper presents the SEDGES model's structure, equations, and ability to simulate ecological and hydrological variables.

The intended main use of SEDGES is to provide atmospheric general circulation models within Earth System models of intermediate complexity a set of land surface variables that vary in line with large scale vegetative and soil properties. That said, SEDGES has been designed, in particular, for coupling with the Planet Simulator, and thus presupposes that the land surface scheme in which it is embedded be similar to that of PlaSim in its hydrology and scheme for surface evaporation. SEDGES can also be forced offline with external data. The offline mode was used in combination with reanalysis climate data for the SEDGES model evaluation.

2 Model Description: SEDGES

The main purpose of this simple dynamic global vegetation model is to predict large-scale land surface properties, vegetative productivity, and biomass. This section presents, in detail, the SEDGES model formulations for its output ecological and land surface variables, including their derivations.

2.1 Overview of SEDGES

SEDGES is designed to couple with the Planet Simulator GCM, which uses a bulk aerodynamic formulation with a single tile (i.e. one surface type per grid cell). SEDGES handles sub-grid scale heterogeneity according to what is called the "average parameter" method (Giorgi and Avissar, 1997) or the "composite" approach (Li and Arora, 2012; Melton and Arora, 2014), in which land surface characteristics are aggregated to provide a single, representative value at the scale of the entire grid cell. The framework for evapotranspiration (ET) is special, because it also qualifies as a simplified mosaic (or "mixed" (Li and Arora, 2012)) approach, such that only surface conductance differs between the surface types (or tiles). This mosaic approach is also used to extend a "big leaf" formulation for vegetative CO_2 uptake (Appendix B of Raupach, 1998) to a mixed soil-vegetation surface, enabling us to isolate the fraction of total ET that is due to transpiration and thus formulate vegetative control over water loss and CO_2 uptake. The SEDGES framework neglects evaporation from intercepted canopy water and thus only distinguishes between two tiles when snow is absent: bare soil and vegetation. When there is snow cover, there are essentially three tiles: snow-free exposed bare soil, snow-covered surface, and snow-free exposed vegetation (see section 2.3.3

Geosci. Model Dev. Discuss., doi:10.5194/gmd-2017-75, 2017
Manuscript under review for journal Geosci. Model Dev.
Discussion started: 5 May 2017

Geoscientific Model Development Discussions

for more detail). Overall, SEDGES's handling of sub-grid scale heterogeneity is similar to that of the SLAM-1T configuration of the CHASM model (Desborough, 1999) and of the original MOSES land surface scheme (Cox et al., 1999).

The core driving variable in SEDGES is gross primary productivity (GPP), which impacts the living biomass, which, in turn, heavily influences or determines the values of almost every other simulated land surface variable (listed in section 3). Forest cover and leaf cover fractions and (implicitly) rooting depth are parameterized to increase with biomass using respective relationships that are fixed. SEDGES (as well as SimBA) uses a simple single layer bucket for the soil hydrology and has essentially one plant functional type. Soil carbon is treated as a single homogeneous reservoir. Surface albedo depends on soil carbon content, snow depth, biomass, and leaf cover fraction. Surface roughness increase monotonically with biomass. Gross primary productivity and canopy resistance[1] are coupled through the vegetation's effort to conjointly minimize water loss and satisfy photosynthetic demand for CO_2, as per the original Dewar (1997) model (see section 2.2.6). Table 2 lists all SEDGES variables and their units. How those variables are updated and their dependencies are shown in Figs. 15 and 16. Table 1 lists all parameters that are used in the paper, their values, and their units.

2.2 Equations for Ecological Variables

2.2.1 Vegetation Biomass

The most important SEDGES variable is biomass of live vegetation. This quantity is used to directly or indirectly derive almost all the land surface variables. The prognostic equation for biomass is as follows:

$$\frac{\mathrm{d}C_{veg}}{\mathrm{d}t} = NPP - L, \tag{1}$$

where C_{veg} is the carbon in living biomass $\mathrm{kgC\ m^{-2}}$, L is the litterfall and equals $\frac{C_{veg}}{\tau_{veg}}$, τ_{veg} is the residence time of the vegetative carbon (see section 2.2.7) and equals 10 years, and NPP (net primary productivity) is approximated as $0.5GPP$, where GPP is gross primary productivity.

2.2.2 Net Primary Productivity and Gross Primary Productivity

SEDGES uses a constant $NPP/GPP = 0.5$ approximation. This approximation is supported by the conservative nature of the ratio of mitochondrial respiration to gross photosynthesis and (hence) of the ratio of net photosynthesis to gross photosynthesis over a wide variety of conditions, on time scales of weeks or more (see the brief review in Van Oijen et al. (2010)). Since each model time step in SEDGES is much shorter than this, it thus might seem incorrect to hold NPP/GPP fixed for each time step. It is appropriate to do so, however, because the NPP to GPP ratio in SEDGES only impacts biomass changes, and the latter occur on very long time scales. Finally, meta-analyses on previous studies have found a robust (DeLucia et al., 2007; Litton et al., 2007) linear or proportional relationship between NPP and GPP, with slope or proportionality constant of around

[1]Canopy resistance and conductance are aggregated or "bulk" versions of, respectively, stomatal resistance and conductance, such that the entire canopy can be treated like a big leaf (e.g., see Jarvis and McNaughton, 1986; Raupach and Finnigan, 1988)

Geosci. Model Dev. Discuss., doi:10.5194/gmd-2017-75, 2017
Manuscript under review for journal Geosci. Model Dev.
Discussion started: 5 May 2017

Geoscientific Model Development Discussions
Open Access
EGU

Table 1. SEDGES parameters in the paper.

symbol	value	units	description	source(s)
τ_{veg}	10	years (converted into seconds)	biomass residence time	SimBA (all versions)
R_d	287.0	$\mathrm{J\,K^{-1}\,kg^{-1}}$	gas constant for dry air on Earth	-
ϵ_{max}	5.0×10^{-10}	$\mathrm{kgC\,J^{-1}}$	max. light use efficiency	model calibration
CO_{2comp}	40	ppmv	$\mathrm{CO_2}$ light compensation point	Franks et al. (2013)
T_{crit}	20	$^{\circ}\mathrm{C}$	temperature at which productivity limitation begins	see section 2.2.3
k_{veg}	1	-	light extinction coefficient	see section 2.2.3
Ω_c	0.7	-	clumping index	Pisek et al. (2010); He et al. (2012)
$co2conv$	4.15×10^{-7}	$\mathrm{kgC\,kgair^{-1}\,ppmv^{-1}}$	unit conversion factors	manipulation of equation B7 from Raupach (1998)
$\frac{c_i}{c_a}$	0.80	-	ratio of intercellular to atmospheric $\mathrm{CO_2}$	somewhat common daytime value for C3 plants
$r_{ss}min$	10	$\mathrm{s\,m^{-1}}$	minimum soil surface resistance	van de Griend and Owe (1994)
$r_{ss}max$	10^{30}	$\mathrm{s\,m^{-1}}$	maximum soil surface resistance	-
ρ_w	1000	$\mathrm{kg\,m^{-3}}$	density of liquid water	-
$f_{snowfor}$	0.12	-	snow-covered fraction of the forest cover	see section 2.2.5
$trmax$	2.78×10^{-7}	$\mathrm{m\,s^{-1}}$	max. transpiration rate	Knorr (2000)
r_cmin_{min}	0	$\mathrm{s\,m^{-1}}$	absolute min. canopy resistance	-
r_cmax	10^{30}	$\mathrm{s\,m^{-1}}$	max. canopy resistance	Sitch et al. (2003)
c_8	$\approx$ 43.3 (see section 2.2.7)	-	for normalizing 10 $^{\circ}$C soil respiration to that of SimBA	
c_9	106	K	for soil respiration	Jenkinson et al. (1990)
LAI_{min}	0.05	-	min. leaf area index in wet soils	-
LAI_{max}	7	-	max. leaf area index in wet soils	model calibration
c_6	0.195	$\mathrm{kgC^{-1}\,m^2}$	biomass to LAI conversion	model calibration
$W_{frac_{crit,lai}}$	0.05	-	critical soil wetness fraction for commencement of leaf fall	model calibration
c_1	0.2	$\mathrm{kgC^{-1}\,m^2}$	biomass-forest cover relationship	see section 2.2.9
c_2	1.0	$\mathrm{kgC\,m^{-2}}$	biomass threshold for forest cover commencement	see section 2.2.9
c_7	9	$\mathrm{kgC\,m^{-2}}$	soil carbon saturation value with respect to soil albedo	see section 2.3.1
α_{sand}	0.32	-	sandy soil albedo	see section 2.3.1
α_{peat}	0.12	-	albedo of organic matter-rich soil	see section 2.3.1
c_4	1.5	$\mathrm{kgC^{-1}\,m^2}$	shape parameter for snow-covered albedo	model calibration
c_5	1.5	$\mathrm{kgC\,m^{-2}}$	biomass threshold for snow masking	model calibration
$\alpha_{mindeepsnowflat}$	0.40	-	albedo of warm, deep, pure snow	Roesch et al. (2001)
$\alpha_{maxdeepsnowflat}$	0.80	-	albedo of cold, deep, pure snow	Roeckner et al. (2003)
$\alpha_{maxsnowfor}$	0.30	-	maximum albedo of snow-covered forest	Moody et al. (2007)
c_{12}	0.10	$\mathrm{kgC}^{\frac{1}{2}}$	conversion of biomass into soil bucket depth	model calibration
$W_{max\,min}$	0.05	m	minimum soil bucket depth	see section 2.3.2
z_{0min}	0.01	m	surface roughness for bare soil	Oke (1987)
z_{0const}	$\approx$ 0.035	m	biomass-roughness relationship	see section 2.3.3
c_{15}	8	$\mathrm{kgC\,m^{-2}}$	biomass-roughness relationship	model calibration
c_{16}	0.5	$\mathrm{kgC^{-1}\,m^2}$	biomass-roughness relationship	model calibration
c_{17}	2.5	m	$\approx$ surface roughness for fully-forested land	typical value for tropical rainforests (Sellers et al., 1996)

0.5 (Gifford, 2003; DeLucia et al., 2007; Litton et al., 2007), albeit with considerable variation in NPP/GPP across field sites (Amthor and Baldocchi, 2001; DeLucia et al., 2007; Litton et al., 2007).

GPP is calculated as the minimum of a light-limited rate, GPP_L, and a water-limited rate, GPP_W (Monteith et al., 1989; Dewar, 1997). That is, $GPP = min(GPP_L, GPP_W.)$

Geosci. Model Dev. Discuss., doi:10.5194/gmd-2017-75, 2017
Manuscript under review for journal Geosci. Model Dev.
Discussion started: 5 May 2017

Geoscientific Model Development Discussions
Open Access
EGU

Table 2. SEDGES variables in the paper.

symbol	units	description
C_{veg}	$\mathrm{kgC\ m^{-2}}$	vegetative carbon
L	$\mathrm{kgC\ m^{-2}\ s^{-1}}$	litterfall
NPP	$\mathrm{kgC\ m^{-2}\ s^{-1}}$	net primary productivity
GPP	$\mathrm{kgC\ m^{-2}\ s^{-1}}$	gross primary productivity
GPP_L	$\mathrm{kgC\ m^{-2}\ s^{-1}}$	light-limited gross primary productivity
GPP_W	$\mathrm{kgC\ m^{-2}\ s^{-1}}$	water-limited gross primary productivity
$f_1(CO_2)$	-	CO_2 fertilization function
$f_2(T_{sfc})$	-	temperature limitation function
T_{sfc}	K	surface temperature
f_{APAR}	-	fraction of photosynthetically active radiation (PAR) that is absorbed by green vegetation
$SW\downarrow$	$\mathrm{W\ m^{-2}}$	surface downwelling short wave radiation
LAI	$\mathrm{m^2\ leaf\ area\ (m^2\ ground\ area)^{-1}}$	leaf area index
f_{veg}	-	fractional green vegetation (leaf) cover
g_a	$\mathrm{m\ s^{-1}}$	aerodynamic conductance
r_a	$\mathrm{s\ m^{-1}}$	aerodynamic resistance
r_c	$\mathrm{s\ m^{-1}}$	canopy resistance
ρ	$\mathrm{kg\ m^{-3}}$	surface air density
p_{sfc}	Pa	surface pressure
ET	$\mathrm{m^3\ m-2s^{-1}}$	evapotranspiration
$qsat_{sfc}$	$\mathrm{kgH_2O\ kgair^{-1}}$	surface saturation specific humidity
q	$\mathrm{kgH_2O\ kgair^{-1}}$	specific humidity at the lowest atmospheric level
C_w	-	surface wetness factor
β_{ss}	-	soil surface water stress factor
r_{ss}		soil surface resistance
W_{frac}	-	soil wetness fraction
W_{soil}	m	soil water content
W_{max}	m	soil "bucket" depth
T	$\mathrm{m^3\ m-2s^{-1}}$	transpiration
r_{cu*}	$\mathrm{s\ m^{-1}}$	case-specific unconstrained canopy resistance
r_{cu}	$\mathrm{s\ m^{-1}}$	unconstrained canopy resistance
β_{tr}	-	water stress factor for transpiration
r_cmin	$\mathrm{s\ m^{-1}}$	minimum canopy resistance
C_{soil}	$\mathrm{kgC\ m^{-2}}$	soil carbon
R_{soil}	$\mathrm{kgC\ m^{-2}\ s^{-1}}$	soil respiration rate
T_{soil}	K	soil temperature at 0.25m depth
LAI_m	$\mathrm{m^2\ leaf\ area\ (m^2\ ground\ area)^{-1}}$	leaf area index without soil moisture stress
f_{veg_m}	-	fractional green vegetation (leaf) cover in absence of soil moisture stress
$f_{veg_{dry}}$	-	max fractional green vegetation (leaf) cover under soil moisture stress
f_{for}	-	forest cover fraction
α_0	-	snow-free surface albedo
α_{soil}	-	albedo of bare soil
α	-	albedo
$\alpha_{snowflat}$	-	snow-covered albedo of flat portion of grid cell
$\alpha_{snowfor}$	-	snow-covered albedo of forested portion of the grid cell
$f_{snowflat}$	-	fraction of "flat" portion of grid cell that is snow-covered
swe	$\mathrm{m^3\ m^{-2}}$	snow depth in liquid water equivalent
$\alpha_{deepsnowflat}$	-	albedo of deep and pure snow
z_0	m	surface roughness
z_{0oro}	m	surface roughness due to orography
z_{0veg}	m	surface roughness due to vegetation
P	$\mathrm{m^3\ m^{-2}\ s^{-1}}$	precipitation in liquid water equivalent
S	$\mathrm{m^3\ m^{-2}\ s^{-1}}$	snowfall in liquid water equivalent
M	$\mathrm{m^3\ m^{-2}\ s^{-1}}$	snowmelt in liquid water equivalent
ET_{soil}	$\mathrm{m^3\ m^{-2}\ s^{-1}}$	soil evaporation plus transpiration
PET	$\mathrm{m^3\ m^{-2}\ s^{-1}}$	potential evapotranspiration

Geosci. Model Dev. Discuss., doi:10.5194/gmd-2017-75, 2017
Manuscript under review for journal Geosci. Model Dev.
Discussion started: 5 May 2017

Geoscientific Model Development Discussions

Table 3. RMSE's and correlations between annual mean climatologies of SEDGES variables and those for reference datasets

variable	correlation	RMSE	reference dataset	analyzed years
ET	0.778549	0.72505 $\mathrm{mm\ d^{-1}}$	Mueller et al. (2013)	1989-2005
GPP	0.924035	-	MTE (Jung et al., 2011)	1990-2009
GPP	0.861378	-	CARBONES	1990-2009
vegetative carbon	0.570484	3.91639kgC $\mathrm{m^{-2}}$	Olson et al. (1985)	see text
soil carbon	0.579095	7.93438kgC $\mathrm{m^{-2}}$	HWSD v.1.2 (Wieder et al., 2011)	see text

2.2.3 Light-limited Gross Primary Productivity

GPP_L uses a light-use efficiency (LUE) formulation (e.g. see Yuan et al. (2007)). The equation is as follows:

$$GPP_L = \epsilon_{max} \cdot f_1(CO_2) \cdot f_2(T_{sfc}) \cdot f_{APAR} \cdot SW{\downarrow}; \tag{2}$$

where

ϵ_{max} is a globally-constant maximum LUE parameter = 5.0×10^{-10} kgC $\mathrm{J^{-1}}$;
$f_1(CO_2)$ is a CO_2 fertilization function (described below);
$f_2(T_{sfc})$ is a temperature limitation function (described below);
f_{APAR} is the fraction of photosynthetically active radiation (PAR) that is absorbed by green vegetation (see below); and
$SW{\downarrow}$ is the downward flux of shortwave radiation just above the canopy surface (in W $\mathrm{m^{-2}}$).

In Eq. (2), the first term on the right hand side, ϵ_{max}, is the LUE with respect to the total short wave broadband radiation that is absorbed by the photosynthetic parts of the vegetation. This constant term is the maximum efficiency with which incident short wave radiation can be used to synthesize vegetative carbon at the reference (360ppmv) CO_2 level (also see explanation of f_{APAR}, below).

The second term in Eq. (2), $f_1(CO_2)$, increases productivity with increasing CO_2 and is taken directly from Eq. 5 of Franks et al. (2013). For $CO_2 > CO_{2comp}$, we have

$$f_1(CO_2) = CO_{2norm} \frac{c_a - CO_{2comp}}{c_a + 2CO_{2comp}}, \tag{3}$$

where

c_a is the atmospheric CO_2 concentration (ppmv),
$CO_{2comp} = 40$ppmv is the light compensation point in the absence of dark respiration, and
$CO_{2norm} = \frac{360+2CO_{2comp}}{360-CO_{2comp}}$.
Otherwise, $f_1(CO_2) = 0$. This fertilization function replaces an earlier "beta" factor approach used in SimBA (Lunkeit et al., 2011).

Geosci. Model Dev. Discuss., doi:10.5194/gmd-2017-75, 2017
Manuscript under review for journal Geosci. Model Dev.
Discussion started: 5 May 2017

Geoscientific Model Development Discussions

The third term in Eq. (2) is $f_2(T_{sfc})$. $f_2(T_{sfc})$ is a ramp function, reducing productivity linearly from a surface temperature of $T_{crit} \equiv 20$ °C to 0 °C, with $f_2(T_{sfc})$ = 0 for below-0 °C temperatures. The 20 °C value is the critical temperature below which productivity drops. See appendix A for more discussion.

The fourth term in Eq. (2) is f_{APAR}. "f_{APAR}" refers to the fraction of photosynthetically active radiation (PAR) that is absorbed by photosynthesizing parts (i.e. green leaves) of plants. PAR is the portion (≈ 50 %) of incoming solar radiation that is in wavelengths usable for photosynthesis. We approximate f_{APAR} as follows:

$$f_{APAR} = 1 - e^{-k_{veg} \cdot \Omega_c \cdot LAI}, \tag{4}$$

where

k_{veg} is a light extinction coefficient (set to 1 for horizontal leaves),

Ω_c is the clumping index (or factor) and is set to 0.7, a near-mean value for natural land cover types (Pisek et al., 2010; He et al., 2012), and

LAI is the leaf area index (see section 2.2.8).

Equation (4) uses a simple Beer-Lambert approach, extended to canopies with leaves that are non-randomly distributed in space (Nilson, 1971) (e.g. "clumped"). Here, we have used the common approximation (e.g., see Gower et al., 1999) that f_{APAR} equals the fraction of intercepted PAR (f_{IPAR}). Other assumptions and simplifications in Eq. (4) include an azimuthally symmetric leaf distribution (Gower et al., 1999), leaf absorptivity of 1 with respect to PAR, and the neglect of the influence of non-photosynthesizing plant parts. A final and important assumption of horizontal leaves[2] eliminates zenith angle dependency of the light extinction coefficient (Campbell and Norman, 1998), which makes the canopy gap fraction the same from any angle. This, in turn, eliminates the dependency of f_{IPAR} on diffusive/direct radiative partitioning and on zenith angle, thus reducing f_{IPAR} (and f_{APAR}) to the simple Beer-Lambert expression of Eq. (4), with constant light extinction coefficient. Earlier versions of SimBA and the derivative model (Dewar, 1997) assumed a constant value of 0.5 for k_{veg}.

The simplifications made in the last paragraph allow us to interchange f_{APAR} and the vegetative (or leaf) cover fraction, f_{veg}. Thus, we can rewrite Eq. (4) as follows:

$$f_{veg} = 1 - e^{-k_{veg} \cdot \Omega_c \cdot LAI}, \tag{5}$$

where f_{veg} is the areal fraction of view that is covered by photosynthesizing plant parts when looking directly down on the land surface. That is, f_{veg} = 1- the gap fraction from the nadir.

[2]While spherical leaf angle distribution is commonly assumed for unmeasured canopies, measurements of 58 temperate and boreal broadleaf tree species showed planophile (tending toward horizontal) leaf angle distributions in 30 and spherical distributions in just 5 (Pisek et al., 2013). Moreover, a modeling study (Hikosaka and Hirose, 1997) used game theoretical arguments to show how a horizontal leaf angle distribution is to be evolutionarily expected, in general (save for canopies with high LAI and high self-shading). Thus, globally applying a horizontal canopy leaf distribution is not unreasonable.

Geosci. Model Dev. Discuss., doi:10.5194/gmd-2017-75, 2017
Manuscript under review for journal Geosci. Model Dev.
Discussion started: 5 May 2017

Geoscientific Model Development Discussions
Open Access
EGU

2.2.4 Water-limited Gross Primary Productivity

Most land plants take up the CO_2 they need for photosynthesis through tiny pores in their leaves called "stomata". Water is also lost (transpired) through these same openings. Water loss in excess of water uptake can lead to cavitation, hydraulic system collapse (e.g., see discussion in Sperry et al., 2002), and/or permanent reduction in photosynthetic capacity (Lawlor and Cornic, 2002). To prevent and mitigate such occurrences in both the present and future, most land plants adjust their stomatal openings in such a way as to balance the short and long term costs of transpiration with the photosynthetic gain from increased CO_2 intake (Cowan and Farquhar, 1977; Medlyn et al., 2011; Buckley and Schymanski, 2014; Prentice et al., 2014). Thus, water limitation in most land plants is closely tied to CO_2 limitation on photosynthesis. For this reason, we refer to this CO_2-limited rate in SEDGES as the "water-limited rate of GPP". This rate is given as follows:

$$GPP_W = \frac{(co2conv)(1-\frac{c_i}{c_a})c_a(f_{veg})\rho}{1.6r_c + r_a}; \quad (6)$$

where

r_c is the canopy resistance (see section 2.2.6);

r_a is the aerodynamic resistance;

ρ ($\equiv \frac{p_{sfc}}{R_d T_{sfc}}$) is the surface air density, where p_{sfc} is the surface pressure and R_d is the gas constant for dry air;

$co2conv = 4.15 \times 10^{-7}$ kgC kgair^{-1} ppmv^{-1};

c_i represents a "bulk leaf" intercellular concentration of CO_2 (ppmv); and

$\frac{c_i}{c_a}$ is set to 0.80.[3]

Equation (6) is essentially the bulk aerodynamic formula for CO_2 in appendix B of Raupach (1998), except that we have multiplied their right hand side by f_{veg} to generalize from their big leaf approach to the simplified mosaic framework (as mentioned in section 2.1), and we have multiplied by the ratio of the molar masses of carbon and CO_2 to convert the flux into carbon units. In addition, we neglect the contribution of leaf mitochondrial respiration for simplicity. (It can be shown that including daytime leaf mitochondrial respiration in the formulation of GPP_W multiplies its current form by a factor of $\frac{1}{1-X}$, where X is the ratio of leaf mitochondrial respiration under light to gross photosynthesis.)

The above bulk aerodynamic formulation for GPP_W in SEDGES is more realistic than the diffusive scheme used in earlier versions of SimBA and in the Dewar (1997) model. The latter scheme works well at the canopy level only if $r_c >> r_a$. This condition is likely to be satisfied for aerodynamically rough canopies and when using daily-averaged environmental conditions, such as in Dewar (1997). However, early diagnostic tests of SEDGES coupled with PlaSim showed that the condition was often not satisfied, thus motivating our implementation of the bulk aerodynamic formulation for CO_2 uptake. Implementing the new formulation led to higher daytime values of r_c for moist areas. These values were more in line with reported maximum surface conductances for various vegetation types (Kelliher et al., 1995).

[3]This value was lowered from the ≈ 0.86 value that was apparently used in Raupach (1998) because such a high value is less representative of typical daytime $\frac{c_i}{c_a}$ values (e.g., see Prentice et al., 2014). SimBA uses a value of 0.7.

Geosci. Model Dev. Discuss., doi:10.5194/gmd-2017-75, 2017
Manuscript under review for journal Geosci. Model Dev.
Discussion started: 5 May 2017

Geoscientific Model Development Discussions

2.2.5 Evapotranspiration and Transpiration

While SEDGES does not directly calculate evapotranspiration (ET), it provides a surface wetness factor to be used by the bulk aerodynamic formulation of the land surface scheme of the coupled atmospheric model, which calculates ET externally. SEDGES presupposes that the saturation specific humidity of the air at the surface is homogeneous throughout the grid cell:[4]

$$ET = \frac{\rho}{\rho_w \, r_a} C_w \Delta q, \tag{7}$$

where ET is the evapotranspiration in units of volumetric liquid water $\mathrm{m}^3 \ \mathrm{m}^{-2} \ \mathrm{s}{-}1$,

ρ_w is the density of liquid water,

$\Delta q \equiv qsat_{sfc} - q$,

$qsat_{sfc}$ is the temperature- (T_{sfc}) and pressure- (p_{sfc}) dependent saturation specific humidity of the air at the surface,

q is the specific humidity of the air at the lowest atmospheric model level, and

C_w is a surface "wetness" factor that reduces evapotranspiration from the potential rate by incorporating the effects of canopy resistance and soil resistance. C_w ranges from 0 to 1, where "1" gives the potential ET rate.

Although the above framework for ET is required in order for SEDGES to operate as designed, there is no stipulation that the coupled land surface model calculate $qsat_{sfc}$ or r_a in any preset way. That said, it is desirable for the calculation of r_a to depend, in some way, on the surface roughness length that is output by SEDGES 2.3.3.

Under snow-free conditions, SEDGES derives the key ET variable, the surface wetness factor, as follows:

$$C_w = \frac{f_{veg}}{1 + r_c g_a} + \frac{1 - f_{veg}}{1 + r_{ss} g_a}; \tag{8}$$

where

g_a is the aerodynamic conductance ($= \frac{1}{r_a}$)[5], and

r_{ss} is the soil surface resistance, whose formulation is taken from the JULES model (Best et al., 2011), except for the use of the lower minimum soil resistance from van de Griend and Owe (1994). This reduction was made to compensate for the absence of evaporation from ponded surface water in SEDGES. Soil surface resistance is formulated as follows:

$$r_{ss} = min\left(r_{ss}max, \frac{r_{ss}min}{\beta_{ss}}\right), \tag{9}$$

where

[4] In this paper, we define evapotranspiration (ET) and transpiration (T) as positive when there is a net water vapor flux from surface to atmosphere. In the actual SEDGES code, ET and T are defined as negative when the flux is from surface to atmosphere. In our exposition, we have reversed the sign convention to aid interpretation of the model equations.

[5] An important requirement for the aerodynamic conductance formulation is that the surface roughness for moisture be the same as that for momentum. See section 2.3.3 for more discussion.

Geosci. Model Dev. Discuss., doi:10.5194/gmd-2017-75, 2017
Manuscript under review for journal Geosci. Model Dev.
Discussion started: 5 May 2017

Geoscientific Model Development Discussions

$r_{ss}min$ is the minimum soil surface resistance of 10 s m^{-1} (van de Griend and Owe, 1994),
$r_{ss}max$ is the maximum soil surface resistance (a very large number), and
β_{ss} limits evaporation from the soil surface and is considered a "water stress factor". This factor is formulated according to Best et al. (2011), except that SEDGES uses the entire soil hydrological layer instead of just the top of several layers. The water stress factor for the soil surface in SEDGES is as follows:

$$\beta_{ss} = {W_{frac}}^2, \tag{10}$$

where the soil wetness fraction, W_{frac}, is given as follows:

$$W_{frac} = \frac{W_{soil}}{W_{max}}, \tag{11}$$

where W_{max} is the the biomass-dependent soil "bucket" depth and W_{soil} is the water content (as depth) within the bucket. The SimBA model used a general water stress factor that was a ramp function, reducing ET linearly from a soil wetness fraction of 0.5 to 0. In SimBA, C_w was equal to this water stress factor. In this way, no distinction was made between soil moisture's impact on soil evaporation and its impact on transpiration.

Examining Eq. (8), we see that C_w is comprised of a vegetation term and a bare soil term (since $1 - f_{veg}$ is the bare soil fraction). The vegetation term involves loss of water only due to transpiration; canopy interception and evaporation are neglected for simplicity. Under snow-free conditions, ET is partitioned into transpiration and bare soil evaporation, respectively, by replacing C_w in Eq. (7) with the vegetation term, $\frac{f_{veg}}{1+r_c g_a}$ or with the bare soil term, $\frac{1-f_{veg}}{1+r_{ss} g_a}$. Doing so with the vegetation term yields the following equation for transpiration:

$$T = \frac{\rho}{\rho_w} \frac{f_{veg}}{r_a + r_c} \Delta q. \tag{12}$$

From the above formulations, one can see that we weight the contributions to evapotranspiration from transpiration and bare soil evaporation, respectively, by the fractional coverages of vegetation and bare soil.

In the presence of snow cover, the surface is treated as a mosaic of different types, with each type sharing the same aerodynamic conductance, soil hydrology, and surface temperature as before (section 2.1) The parts of the grid cell that are snow-covered evaporate at the potential rate. The snow-free portion is comprised of vegetation parts that protrude above the snow pack and are snow-free, the exposed bare soil, and the exposed, low-lying leaf cover. In these snow-free portions of the grid cell, transpiration is 0, and bare soil evaporation occurs (Eqs. (7), (8), and (9)). The final equation for C_w in the presence of snow in the grid cell is as follows:

$$C_w = \frac{(1 - f_{for})(1 - f_{veg})(1 - f_{snowflat})}{1 + r_{ss} g_a} + (1 - f_{for})(f_{snowflat}) + (f_{for})(f_{snowfor}), \tag{13}$$

Geosci. Model Dev. Discuss., doi:10.5194/gmd-2017-75, 2017
Manuscript under review for journal Geosci. Model Dev.
Discussion started: 5 May 2017

where

f_{for} is the forest cover fraction (Eq. 20),

$f_{snowflat}$ is the fraction of the flat portion of the grid cell that is covered by snow (see Eq. 24 and nearby text), and

$f_{snowfor} \equiv 0.12$ is the snow-covered fraction of the vegetation cover that protrudes above the snow pack (i.e. of the forest cover).[6]

In SimBA, $C_w = 1$ when there is snow cover. The formulation was changed in SEDGES when it was discovered that it led to excessive ET when snow was present. The original MOSES and its progenitor UKMO scheme also set their equivalent C_w to 1 when there is snow cover, which also leads to excessive ET under those conditions (Essery, 1998; Cox et al., 1999).

2.2.6 Canopy Resistance

Canopy resistance, r_c, is determined at each time step in accordance with the supply/demand principle in the original Dewar (1997) paper. That is, the plants attempt to adjust r_c so that CO_2 uptake exactly matches the light-limited rate of canopy photosynthesis, GPP_L. (GPP_L is the rate of gross carbon uptake in the absence of any CO_2 limitation.) However, r_c must also be sufficiently high to prevent transpiration from exceeding the maximum rate suppliable by the roots (the "supply rate"). If the r_c value that would be needed to satisfy the CO_2 demand would cause the transpiration to exceed the supply rate, then water/CO_2 limitation occurs, and r_c takes on the value that would yield transpiration at the supply rate. In the derivation of the equation for canopy resistance, the unconstrained adjustment of r_c is the first step. The second step is the calculation of the minimum possible value of r_c that satisfies the supply constraint on transpiration. If needed, the unconstrained r_c is raised to this minimum value. r_c is also constrained to not exceed a maximum possible value, $r_c max$. Details on the mechanics of the formulation are given in appendix B. The original SimBA model did not explicitly consider canopy resistance.

2.2.7 Soil Carbon

The overall modeling framework for soil carbon is the same as that for the land surface component (ENTS) of the GENIE model (Williamson et al., 2006). In this simple framework, soil carbon is treated as a single homogeneous reservoir (in which litter is included) that has a single, temperature-dependent residence time. Soil respiration (see below) depends only on temperature. The prognostic equation for soil carbon is given by

$$\frac{\mathrm{d}C_{soil}}{\mathrm{d}t} = L - R_{soil}, \tag{14}$$

where

C_{soil} is the soil carbon ($\mathrm{kgC\ m^{-2}}$),

L is the litterfall (Eq. 1), and

R_{soil} is the rate of soil respiration ($\mathrm{kgC\ m^{-2}\ s^{-1}}$).

[6]The value of 0.12 is a crude estimate that is obtained by assuming an albedo transition for forest vegetation from snow-free vegetation albedo to deep and cold snow albedo (0.80) that is linear with $f_{snowfor}$. Depending on whether one uses values of 0.30 and 0.12 for the values of snow-covered forest and snow-free vegetation, respectively, or values taken from Betts and Ball (1997), one ends up with $f_{snowfor}$ values ranging from ≈ 0.04 to 0.26.

Geosci. Model Dev. Discuss., doi:10.5194/gmd-2017-75, 2017
Manuscript under review for journal Geosci. Model Dev.
Discussion started: 5 May 2017

Soil respiration is modeled according to the following equation:

$$R_{soil} = \begin{cases} \frac{c_8 C_{soil}}{\tau_{soil}\left(1+e^{\frac{c_9}{T_{soil}-254.85}}\right)}, T_{soil} > 256.1\,\mathrm{K}, \\ 0, T_{soil} \leq 256.1\,\mathrm{K}, \end{cases} \quad (15)$$

where

T_{soil} is the soil temperature at ≈0.10 m depth,

τ_{soil} is the residence time (42 years) of the soil carbon at 10 °C,

$c_8 \equiv 1 + e^{\frac{106}{283.15-254.85}}$, and

$c_9 = 106\mathrm{K}$.

The above formulation is based on that of ENTS (Williamson et al., 2006), except that we replace its temperature dependency (Lloyd and Taylor, 1994) with that from the RothC soil carbon model (Jenkinson et al., 1990), since the latter's temperature function reduces a negative soil carbon bias in the high Arctic. In addition, we use c_8 as a normalizing constant to make the soil carbon residence time, $\frac{C_{soil}}{R_{soil}}$, at 10 °C the same as in the original SimBA formulation. Moreover, for strictly numerical purposes, 256.1K is used as the cut off temperature, below which soil respiration is set to 0. In the current version of SEDGES, it is tacitly assumed, for simplicity, that all respired soil carbon is emitted directly to the atmosphere.

2.2.8 Leaf Area Index and Leaf Cover Fraction

Leaf area index (LAI) is typically defined as "the one-sided leaf area per unit ground area", or else, for conifers, as the projected area of the needle leaves (Monson and Baldocchi, 2014, p. 246). In SEDGES (as well as in SimBA), LAI is based on a moist soil value that gets subsequently reduced for conditions of low soil moisture. We first describe the moist soil formulation.

For sufficiently moist soils, LAI is a simple function of biomass. In the version of SimBA that came out with version 15 of the Planet Simulator model (Lunkeit et al., 2007), this moist soil LAI was a linear function of forest cover fraction. For SimBA in version 16 of Planet Simulator, the LAI functional dependency on biomass (Lunkeit et al., 2011) was updated to reduce the high number of multiple equilibria in the coupled climate-vegetation system that Dekker et al. (2010) found when using PlaSim version 15. This new parameterization is maintained in SEDGES, but its three parameters have updated values.

The equation for LAI in the absence of soil moisture stress is a monotonically increasing function of biomass with decreasing slope:

$$LAI_m = LAI_{min} + \frac{2}{\pi} LAI_{max} atan(c_6 C_{veg}), \quad (16)$$

where LAI_{min} and LAI_{max} are the minimum and maximum LAI's (respectively) under moist soil conditions. LAI_{min} is set to 0.05 and represents a seeding source with negligible mass. LAI_{max} is set to 7.

Geosci. Model Dev. Discuss., doi:10.5194/gmd-2017-75, 2017
Manuscript under review for journal Geosci. Model Dev.
Discussion started: 5 May 2017

Geoscientific Model Development Discussions

While winter-deciduous phenology is not included in SEDGES, the model simulates drought-deciduous phenology using a crude parameterization from SimBA that came originally from the ECHAM3 model (Klimarechenzentrum, 1993). LAI_m is converted into leaf cover fraction, f_{veg_m} by substituting it into Eq. (5). Then, we set

$$f_{veg} = \min\left(f_{veg_m}, f_{veg_{dry}}\right) \tag{17}$$

where

$$f_{veg_{dry}} = \begin{array}{l} 1, W_{frac} \geq W_{frac_{crit,lai}}, \\ \frac{W_{frac}}{W_{frac_{crit,lai}}}, 0 < W_{frac} < W_{frac_{crit,lai}}. \\ 0, W_{frac} = 0, \end{array} \tag{18}$$

Here, $f_{veg_{dry}}$ represents the maximum leaf cover permitted by the soil wetness fraction; $W_{frac_{crit,lai}}$ is the critical soil wetness fraction at which leaf cover begins to get restricted and is set to 0.05.

The final LAI is only a diagnostic. The f_{veg} in Eq. (17) is converted back into LAI by inverting the LAI_m-$f_{veg_{dry}}$ relationship in Eq. (5) to obtain

$$LAI = \frac{-\ln(1 - f_{veg})}{k_{veg} \cdot \Omega_c}. \tag{19}$$

2.2.9 Forest Cover Fraction

In SEDGES, forest cover fraction helps to determine the amount of surface that is covered by snow for the calculation of evaporation (see Eq. 13). In SimBa, forest cover affected the albedo of snow-covered land; instead, SEDGES has a dependency on biomass. As in the last version of SimBA (Lunkeit et al., 2011), forest cover is parameterized to commence at a biomass of 1 $\mathrm{kgC\ m^{-2}}$. Such cover would represent woody shrubs. Only at a biomass threshold of 1.5 $\mathrm{kgC\ m^{-2}}$ is the woody cover considered tall enough so as to protrude above the winter snow pack and lower the albedo (section 2.3.1). Forest cover fraction is formulated as follows:

$$f_{for} = \max(0, 1 - e^{-c_1(C_{veg} - c_2)}), \tag{20}$$

where c_1 is a shape parameter and c_2 is the biomass threshold for forest cover.

The derivation of the c_1 and c_2 parameter values involved translating NPP from outside data into SEDGES biomass. If one assumes long time scales and steady state conditions, then the translation is readily achieved by setting the left hand side of Eq. (1) to 0, and solving for C_{veg} in terms of NPP. Doing so results in the following relationship: $NPP = \frac{C_{veg}}{\tau_{veg}}$. Using this relationship allows modeled annual NPP from Cramer et al. (1999) and McGuire et al. (1992) to be interpreted as SEDGES biomass equivalent. Then, comparing the real world spatial distribution of boreal forest, boreal woodland, and tundra with the NPP data in those sources, including the NPP ranges for boreal forest, boreal woodland, and tundra ecosystems in McGuire

Geosci. Model Dev. Discuss., doi:10.5194/gmd-2017-75, 2017
Manuscript under review for journal Geosci. Model Dev.
Discussion started: 5 May 2017

Geoscientific Model Development Discussions

et al. (1992), yielded a rough threshold value of 1 $\mathrm{kgC\ m^{-2}}$ for forest cover commencement. The shape parameter, c_1, was tuned so that forest cover fraction values in the Hagemann (2002) land cover dataset would match the NPP values in Cramer et al. (1999) for natural land cover types, while maintaining a fairly close likeness between the SEDGES-parameterized and reference Hagemann (2002) relationships between forest cover fraction and LAI. (This likeness was assessed by scatterplotting the forest cover fraction and maximum LAI for the moist ecosystems given in Hagemann (2002) along with SEDGES-formulated forest cover fractions and LAI's for a wide range of biomass values.) All the previous SimBA formulations gave higher forest cover fractions except for at some low biomass values.

2.3 Equations for Remaining Land Surface Variables

While the equations for the ecological variables were presented in section 2.2, here, we provide the formulations for the land surface variables used by the PlaSim GCM as well as some purely diagnostic variables.

2.3.1 Surface Albedo

A surface albedo with respect to broadband short wave radiation is obtained by incorporating the effects of snow cover on the albedo for snow-free conditions. In obtaining the snow-free albedo (α_0), we simplify by ignoring dependencies on solar zenith angle, diffuse-direct radiation partitioning, the spectral composition of the incident light, the effect of soil moisture on soil albedo, and any impact of leaf litter. Moreover, we neglect variations in leaf reflectivity that often occur between differing plant species and leaf development stages. The formulation of snow-free albedo in SEDGES is of the same form as that for the ECHAM5 GCM (Rechid et al., 2009) and ENTS land surface scheme (Williamson et al., 2006); it is as follows:

$$\alpha_0 = \alpha_{veg} f_{veg} + \alpha_{soil}(1 - f_{veg}), \tag{21}$$

where α_{veg} is the albedo of a completely leaf-covered surface, and α_{soil} is the albedo of the bare soil.

Soil albedo decreases linearly with soil carbon to a minimum value that is reached at 9 $\mathrm{kgC\ m^{-2}}$ and stays constant with further carbon increase. The equation is as follows:

$$\alpha_{soil} = \begin{array}{l} \frac{\alpha_{peat} - \alpha_{sand}}{c_7} C_{soil} + \alpha_{sand}, C_{soil} \leq c_7, \\ \alpha_{peat}, C_{soil} > c_7, \end{array} \tag{22}$$

where

c_7 = 9 $\mathrm{kgC\ m^{-2}}$ and is the soil carbon level at which the soil albedo saturates,

α_{sand} is the soil albedo in the complete absence of soil carbon, and

α_{peat} is the albedo of soil when saturated with soil carbon. This soil albedo formulation is taken from ENTS (Williamson et al., 2006), except for the following modifications: the peat albedo has been increased from 0.11 to 0.12, the sand albedo has been increased from 0.30 to 0.32, and c_7 was decreased from 15 to 9 $\mathrm{kgC\ m^{-2}}$. The first change was made for the sake of model

Geosci. Model Dev. Discuss., doi:10.5194/gmd-2017-75, 2017
Manuscript under review for journal Geosci. Model Dev.
Discussion started: 5 May 2017

Geoscientific Model Development Discussions

simplicity (since the albedo of a fully-leaved surface is 0.12 in SEDGES); the increase in sand albedo was made to better match observed values in the Sahara and Arabian deserts (e.g., Knorr and Schnitzler, 2006). A saturation level for soil albedo as a function of soil column carbon content was estimated to be around 9 $\mathrm{kgC\ m^{-2}}$ by visually comparing the soil/litter surface albedo map from Houldcroft et al. (2009) with a global gridded dataset of soil carbon content (Wieder et al., 2011). Using this estimate for saturation value in SEDGES reduces a positive albedo bias in the high arctic in summer as compared to using the standard ENTS value of 15 $\mathrm{kgC\ m^{-2}}$.

The soil albedo formulation in SEDGES is an advent to SimBA, which has always used a fixed soil albedo of 0.30. The new dynamic scheme was adopted, in part, due to the important role played by ground albedo in Sahelian/Saharan vegetation-precipitation feedbacks, as seen through its effect on low frequency precipitation variability (Vamborg et al., 2014) and increased greening in the mid Holocene (Vamborg et al., 2011). The new scheme also gives more realistic snow-free albedo values in the high latitudes and in the hot deserts (Fig. 11. While the above formulation for snow-free albedo, α_0 neglects, for simplicity, the radiative impact of non-photosynthesizing plant parts (e.g. stems and branches), this impact becomes important (although implicit) in the snow-covered formulation.

A new snow albedo scheme for SEDGES replaces the version from SimBA that linearly combines the albedos from the forested and flat portions of the grid cell according to the forest cover fraction. The SimBA formulation did not simulate well the sharp, real-world transition in snow-covered albedo from tundra to boreal forest (Loranty et al., 2014), which is why a new exponential decay scheme was developed.

In SEDGES, for snow depth > 0, the surface is treated as consisting of two components: 1) "flat" surface (consisting of exposed soil, prostrate vegetation, and dwarf shrubs) that can be partially or entirely buried by the snow cover; 2) "forest" that is covered by trees and shrubs of sufficient stature as to protrude above the snow pack and mask it from the sun via their leaves, stems, and/or branches, regardless of accumulated snow depth on the ground. A non-linear combination of the albedo of the flat portion and the snow-covered forest albedo yields the final surface albedo (α):

$$\alpha = (\alpha_{snowflat} - \alpha_{snowfor}) e^{-c_4 \cdot max(0, C_{veg} - c_5)}, \tag{23}$$

where

c_4 is a shape parameter, and

c_5 is the biomass threshold (1.5 $\mathrm{kgC\ m^{-2}}$) at which the woody vegetation is sufficiently tall as to begin to mask the snow.

Albedo of the flat portion of the grid cell, $\alpha_{snowflat}$, is formulated according to the same temperature dependency (Roeckner et al., 2003) and snow cover fraction (Roesch and Roeckner, 2006) schemes for non-forested areas in the ECHAM5 model, except that we maintain the melting snow albedo of 0.4 from PlaSim and ECHAM4 (Roesch et al., 2001), and we neglect the impact of sloping terrain. We thus have the following:

$$\alpha_{snowflat} = \alpha_0 + (\alpha_{deepsnowflat} - \alpha_0) \cdot 0.95 f_{snowflat}, \tag{24}$$

where

Geosci. Model Dev. Discuss., doi:10.5194/gmd-2017-75, 2017
Manuscript under review for journal Geosci. Model Dev.
Discussion started: 5 May 2017

swe is the snow depth in liquid water equivalent ($\mathrm{m}^3\ \mathrm{m}^{-2}$),

$f_{snowflat} \equiv \tanh(100swe)$ is the fraction of the flat portion of the grid cell that is covered by snow[7],

$\alpha_{deepsnowflat}$ is the albedo of a deep and pure snow pack and is temperature dependent. This dependency has the form of a ramp function, with a maximum albedo, $\alpha_{maxdeepsnowflat} \equiv 0.8$, for surface temperatures $\leq$ -5°C and a minimum albedo, $\alpha_{mindeepsnowflat} \equiv 0.4$, at melting point. These values are the same as in PlaSim and SimBA, except that they have maximum albedo attainment at -10°C.

The albedo of the forest component of the grid cell when there is snow cover is as follows:

$$\alpha_{snowfor} \equiv min(\alpha_{snowflat}, \alpha_{maxsnowfor}). \tag{25}$$

Here, $\alpha_{maxsnowfor}$ is the maximum snow-covered albedo for forest and is set to 0.30, a mid-range white sky albedo value for the different forest types (Moody et al., 2007). Restricting $\alpha_{snowfor}$ to not exceed $\alpha_{snowflat}$ is done because the lower snow depth and warmer snow that reduce the albedo of the flat area also lower the albedo of the forested area to at least the level of the flat area.

2.3.2 Soil Bucket Depth

We first introduced the soil bucket depth, W_{max}, in section 2.2.5 in Eq. (11). SEDGES uses a simplified version of the parameterization in the JeDi dynamic global vegetation model (Pavlick et al., 2013). The JeDi model uses a pipe representation of the rooting system (Shinozaki et al., 1964) in which a square root relationship emerges between W_{max} and coarse root biomass as a result of an assumed constant density of fine roots in the rooting zone. To adapt this formulation to SEDGES, we further assume that coarse root biomass is a fixed fraction of total biomass and that the unit plant available water capacity is spatially constant. Doing so gives the following relationship:

$$W_{max} = \min\left(W_{maxmin}, c_{12}\sqrt{C_{veg}}\right) \tag{26}$$

where c12 is a tuning parameter set to 0.10 $\mathrm{kgC}^{\frac{1}{2}}$. This value yields soil bucket depths that are a reasonably good fit with a plant available water dataset based on optimal rooting depths (Kleidon and Heimann, 1998; Hall et al., 2006; Kleidon, 2011). In that dataset, the soil bucket depths in the most sparsely-vegetated regions range from around 0.05m in the Canadian polar desert to < 0.003m in the hyper-arid Atacama and northeast Sahara deserts. SEDGES adopts a minimum soil bucket depth, W_{maxmin}, of 0.05m.

2.3.3 Surface Roughness

SEDGES has been designed for use by land surface schemes for which the surface roughness lengths for momentum and water vapor are the same (e.g., schemes that use parameterizations from Louis, 1979; Louis et al., 1982). As such, SEDGES returns

[7]Roesch and Roeckner (2006) include the 0.95 multiplier in their definition of the snow-covered fraction of the non-forested part of the grid cell, but we do not.

Geosci. Model Dev. Discuss., doi:10.5194/gmd-2017-75, 2017
Manuscript under review for journal Geosci. Model Dev.
Discussion started: 5 May 2017

Geoscientific Model Development Discussions

only a single value for surface roughness length, z_0, for a grid cell. The (total) surface roughness is comprised of a surface roughness due to orography and a surface roughness due to vegetation:

$$z_0 = \sqrt{{z_{0veg}}^2 + {z_{0oro}}^2}, \tag{27}$$

where z_{0oro} is the orographic surface roughness, and z_{0veg} is the roughness due to vegetation. z_{0oro} is used by some GCM's (including Planet Simulator) to account for the enhancement of surface drag due to sub-grid scale topographic variation (e.g., see Beljaars et al., 2004). z_{0oro} is set to zero by default, because small-scale orographic variation has little effect on land-to-atmosphere moisture transfer (Huntingford et al., 1998; Blyth, 1999).

In the SimBA formulation, surface roughness due to vegetation is parameterized assuming that only forest cover increases it appreciably and that prostrate vegetative cover does not. As such, sparsely-vegetated surfaces are assigned too high of a surface roughness. SimBA has minimum and maximum values of z_{0veg} of $0.05\mathrm{m}$ and $2\mathrm{m}$, respectively (Kleidon, 2006b; Lunkeit et al., 2007, 2011). SEDGES replaces SimBA's linear dependency of z_{0veg} on forest cover fraction with the following logistic curve that depends on biomass rather than forest cover fraction:

$$z_{0veg} = \frac{c_{17}}{1 + e^{-c_{16}(C_{veg} - c_{15})}} - z_{0const}, \tag{28}$$

where

$z_{0const} \equiv \frac{c_{17}}{1+e^{-c_{16}(-c_{15})}}$ is a constant (in m) that forces z_{0veg} to equal z_{0min} at zero biomass. The new formulation for z_{0veg} is tuned by adjusting c_{15} and c_{16} so as to roughly match reference values in the literature for different land cover types (especially those in Hagemann, 2002). z_{0min} is set to a bare soil value of 0.01 m (Oke, 1987). c_{17} represents the approximate maximum value of z_{0veg} and is assigned a value of 2.5 m, which is representative of tropical rainforests (Sellers et al., 1996). z_{0veg} values that lie between these two extremes have been constrained by using the NPP-biomass relationship described in section 2.2.9 and by visually comparing reference NPP and GPP values (Cramer et al., 1999; Jung et al., 2011), biome/land cover distribution maps (Ramankutty and Foley, 1999; Olson et al., 2001), and the aforementioned literature values of z_{0veg} for those land cover types.

3 How to Couple SEDGES

At minimum, the following time-varying input fields are required by SEDGES: aerodynamic conductance (g_a), surface temperature (T_{sfc}), surface downwelling (broadband) short wave radiation ($SW\downarrow$), soil temperature at ≈ 0.25 m (T_{soil}), (bulk aerodynamic) potential evapotranspiration (PET), soil moisture content (W_{soil}), surface pressure (p_{surf}), and snow depth water equivalent (swe). Most of these variables are calculated by full-fledge land surface schemes.

The simulations of aerodynamic conductance, evapotranspiration, and soil moisture content require further input variables than those listed in the previous paragraph. This is also the case when using ERA-Interim reanalysis data to force SEDGES

Geosci. Model Dev. Discuss., doi:10.5194/gmd-2017-75, 2017
Manuscript under review for journal Geosci. Model Dev.
Discussion started: 5 May 2017

Geoscientific Model Development Discussions

(section 4). In addition, the following parameter values (see table 1) are not specified within the actual SEDGES code, which means that they must be declared and assigned values either in outside modules or by modifying the current SEDGES code: maximum light use efficiency (ϵ_{max}), atmospheric CO_2 concentration (c_a), the gas constant for dry air (R_d), maximum transpiration rate ($trmax$), and residences times for vegetative and soil carbon at 10 °C (τ_{veg} and τ_{soil}). SEDGES returns the following output fields: live vegetative biomass (C_{veg}), soil carbon (C_{soil}), soil water holding capacity (W_{max}), surface wetness factor (C_w), transpiration (T) (as a diagnostic), canopy resistance (r_c), surface albedo (α), total surface roughness (z_0), forest cover fraction (f_{for}), leaf area index (LAI), leaf cover fraction (f_{veg}), net primary productivity (NPP), light-limited gross primary productivity (GPP_L), and water-limited gross primary productivity (GPP_W).

In general, the land surface modeling framework that SEDGES presupposes must be reconciled with that of the land surface scheme of the model that one is coupling to. In particular, in the absence of modification to either SEDGES or the external land surface scheme, the simulation of evapotranspiration according to the simplified mosaic and bulk aerodynamic formulations described in sections 2.1 and 2.2.5 is required. The requirement arises because the water and CO_2 exchanges predicted through this framework are presupposed by the canopy resistance equations. The simplest and recommended scenario with regards to reconciling soil hydrology is that the land surface scheme use a single layer bucket model, because this is what SEDGES "sees" when calculating soil surface and canopy resistances. As an example, Eq. (29), used in our forcing of SEDGES with ERA-Interim data (section 4), gives the standard hydrological formulation for the simple single layer bucket model.

In the likely scenario that the land surface scheme of the external model does not perfectly match the framework used by SEDGES, it should, in many cases, be easy to achieve consistency of frameworks by adapting SEDGES and/or the external land surface scheme. Such adaptation would be easiest for the case in which the land surface scheme uses a single or multiple tile/mosaic approach, because this approach could be converted to the simplified mosaic framework of SEDGES by, at each time step, replacing tile surface temperatures and soil wetness fractions with their respective grid cell weighted averages, and by computing an effective surface roughness for the grid cell (e.g., Mason, 1988) in the case of significant areal water body coverage. Finally, many land surface schemes distinguish between a surface roughness length of water vapor and heat from a surface roughness length of momentum, which is done to correct the typical bulk aerodynamic formulation for its replacement of temperature at the height of the roughness length with surface temperature (e.g., see discussion and references in Chen et al., 1997). Although SEDGES only computes a roughness length of momentum, there are many ways to convert this roughness length to the roughness length for vapor/heat (e.g., see analyses and references in Chen et al., 2010).

An advantage of SEDGES is that it can be run at any horizontal and temporal resolution. However, we encourage users to run the model using a sub-daily time step so that the generally positive diurnal covariances of light, temperature, aerodynamic conductance, and surface-to-air specific humidity difference can be adequately captured. These covariances should increase ET, overall. On the other hand, If users choose a daily time step or longer, then they should also anticipate an increase in vegetative productivity in water-limited regions due to the concomitant reduction in water stress. This reduction in water stress can be offset by decreasing $trmax$, the maximum transpiration parameter (appendix B).

Geosci. Model Dev. Discuss., doi:10.5194/gmd-2017-75, 2017
Manuscript under review for journal Geosci. Model Dev.
Discussion started: 5 May 2017

Geoscientific Model Development Discussions

4 Forcing SEDGES with ERA-Interim Reanalysis Data

In order to evaluate the performance of SEDGES, repeated 1981-2010 6-hourly data from the ERA-Interim reanalysis (Dee et al., 2011) is used as the driver. The following required forcing variables (section 3) were obtained from the reanalysis: surface (skin) temperature, surface downwelling short wave radiation, temperature of the second-from-top soil layer, surface pressure, snow depth water equivalent, and the lowest atmospheric model level's specific humidity. We simulate the aerodynamic conductance using these additional variables: the u and v wind components and temperature, all from the lowest atmospheric model level. The aerodynamic conductance is simulated as in the Planet Simulator model (Lunkeit et al., 2011). Soil moisture content is simulated using three additional variables: precipitation, snowfall, and snow melt. Short wave downwelling surface radiation is derived as follows: 3-hourly periods are isolated, and the two periods that straddle each given time (e.g. 12z straddled by the 09z-12z and 12z-15z periods) are averaged to give the flux at that time. A glacier mask is derived by considering any land point that has a daily mean snow depth always greater than zero to be glaciated. No vegetation occurs on glaciated grid points. Finally, all ERA-Interim data are interpolated to T62 resolution using Climate Data Operators (CDO) before being read into SEDGES.

Soil moisture content is simulated as a prognostic variable. As we recommend above in section 3, we use a single layer bucket model, with bucket depth determined by SEDGES. The bucket model is simple. As such, runoff is from the surface and only occurs when the soil moisture content exceeds the bucket depth. Infiltration of liquid water from rainfall and from snow melt is unrestricted. We use the discretized version of the following formulation to simulate soil moisture:

$$\frac{\Delta W_{soil}}{\Delta t} = P - S + M - ET_{soil}, \tag{29}$$

where P is precipitation, S is the rate of snowfall, and M is the rate of snow melt (all in liquid water equivalent). Again, W_{soil} cannot be greater than W_{frac}, with any excess going into runoff. Here, ET_{soil} is the combined soil evaporation and transpiration (and thus not coming from the snow cover). When there is snow cover, we parameterize soil evaporation in line with Eq. (13), so it is thus $\frac{(1-f_{for})(1-f_{veg})(1-f_{snowflat})}{1+r_{ss}g_a} ET$.

Soil hydrology requires careful treatment in the presence of non-zero snow depths. Such care is especially needed because of the tile-based TESSEL land surface scheme that is used by ERA-Interim and the data interpolation to the coarse T62 grid. The underlying TESSEL tile scheme and the spatial interpolation imply that data for a given grid cell that is fed into SEDGES can be physically inconsistent in the SEDGES framework (section 2). The inconsistency arises because a grid cell can have a non-zero snow depth and yet have a homogeneous (as required and seen by SEDGES) surface temperature that is well-above 0 °C. This situation, in the absence of any modification to the SEDGES code, gives rise to common occurrences in which substantial transpiration is occurring from snow-covered leaves and in which snow-covered vegetation and ground are evaporating as if their surface temperatures were well above freezing. These occurrences are not only unphysical; they give rise to higher simulated ET from a given snowy, above-freezing region than would occur over the same region if it were divided up into its original small, homogeneous but differing tiles.

Geosci. Model Dev. Discuss., doi:10.5194/gmd-2017-75, 2017
Manuscript under review for journal Geosci. Model Dev.
Discussion started: 5 May 2017

Geoscientific Model Development Discussions

A second issue that must be addressed when there is snow is the tendency for ERA-Interim to over-predict freezing rain at the expense of snowfall (Dutra et al., 2011). Because we treat rain as entering the soil without interception by the snow pack (as is done in the TESSEL land surface model (Dutra et al., 2010)), the freezing rain bias led our early simulations to have unrealistically large recharge of soil water reservoirs in winter in many locations, even though surface temperatures were well below 0 °C. Handling of the aforementioned snow-temperature inconsistency and the freezing-rain bias are discussed next.

In order to simply resolve the above issue of snow with above-freezing temperature, we separate possible conditions into two cases: 1) $swe > snowthresh$ and 2) $swe \leq snowthresh$, where we define $snowthresh$ as the swe threshold above which the surface is treated as snow-covered with respect to evaporation from and physiology of vegetation and the threshold at or below which the surface is treated as snow-free. In case 1, we assume that transpiration is negligible (due to combined cold temperature and physical coverage of leaves by snow) and thus introduce a slight modification to Eq. (2), by setting $f_2(T_{sfc})$ to 0 (its value at freezing), which, in turn, forces the productivity to 0. In case 2, we assume that evaporation from snow is negligible, and $f_2(T_{sfc})$ is as normal. Finally, we address the excessive partitioning of precipitation into liquid form at subfreezing temperatures by further assuming for case 1 that soil moisture cannot increase unless there is some snow melt during the same time step. Snow melt indicates the presence of above-freezing temperatures and, thus, the presence of liquid water that does not freeze on contact with the surface and can thus infiltrate into the soil.

5 Model Evaluation

SEDGES forced with ERA-Interim reanalysis data is evaluated, with emphasis on the results from the simulation forced with historical CO_2, using reference datasets of vegetative carbon, LAI, surface albedo, tree cover fraction, soil carbon, GPP, and evapotranspiration.

Four simulations are carried out: three equilibrium simulations and one transient simulation. In the three equilibrium simulations atmospheric CO_2 levels of 280, 360, and 560ppm, respectively, are held fixed through the simulations. The vegetation is spun up from a vegetative- and soil carbon-free state. The spin up includes an acceleration of the carbon cycle for the first 260 years(only). From simulation year 261 to year 1500, the carbon cycle is run normally. The model is very nearly at equilibrium by the last 30 years in all three runs, and these years are thus analyzed. The transient simulation begins with the end state of the 280ppm equilibrium simulation and is subsequently forced using observed, transient atmospheric CO_2 values from 1832 to 2010. The CO_2 data is taken from the Mauna Loa dataset (Keeling et al., 1976) for 1959 and on and from 20 year-smoothed ice core data (Etheridge et al., 1998) for the prior years. Unless stated explicitly, the results and analyses always refer to the transient CO_2 simulation. The model performs reasonably well, overall; GPP is simulated exceptionally well.

5.1 Evaluation of Productivity

GPP that is simulated by reanalysis-forced SEDGES is evaluated against two observation-based datasets: MTE (Jung et al., 2011) and CARBONES. In addition, we use the model intercomparisons of (Sitch et al., 2008), (Piao et al., 2013), Anav et al.

Geosci. Model Dev. Discuss., doi:10.5194/gmd-2017-75, 2017
Manuscript under review for journal Geosci. Model Dev.
Discussion started: 5 May 2017

Geoscientific Model Development Discussions

(2015) and modeling-based results of Hemming et al. (2013) and Holden et al. (2013) to assess the relative performance of SEDGES.

For the 1982-2008 period, SEDGES simulates a global mean annual GPP of 126 $\mathrm{PgC\ yr^{-1}}$ as compared to 120 $\mathrm{PgC\ yr^{-1}}$ for the observation-based MTE dataset (Jung et al., 2011). Zonal means of GPP, taken over the glacier-free land mask obtained from the ERA-Interim data and for 1990-2009, are shown for SEDGES, MTE, and the CARBONES data assimilation dataset in Fig. 1. SEDGES captures the large scale patterns very well. Compared to the two reference datasets, SEDGES has positive productivity biases in most of the Southern Hemisphere and around 35 °N, and it has negative biases near the equator and in the high northern latitudes. Moving to the full spatial field, we can see in Fig. 2 that the annual mean GPP, for 1990-2009, in SEDGES and MTE compares very well, overall, with those of MTE and CARBONES. Regionally, as compared to the two reference datasets, SEDGES simulates too high GPP in western Argentina, non-desertic tropical Africa, around the Korean Peninsula, the southwestern and eastern Australian coasts, and too little GPP in almost all the equatorial tropics and Amazonia (see section 5.6 for discussion), the Pacific northwest of the United States, northwestern Europe, and in parts of north-central and far eastern Siberia. In Siberia, SEDGES simulates too low GPP in a dry region northeast of the Kolyma Mountains. This underestimate may be partially due to SEDGES's neglect of leaf mitochondrial respiration in the light, which has been found to be a large fraction (up to ≈ 0.3) of gross photosynthesis in Arctic tundra plants (McLaughlin et al., 2014; Heskel et al., 2014). Indeed, a fraction of 0.3 would, under purely water-limited conditions, increase GPP by 43%.

The spatial correlations between SEDGES and the reference datasets are as high as can be expected (table 3). Spatial correlations between annual mean climatologies of GPP from MTE and three offline land surface models (ORCHIDEE, JULES, and CLM4CN) range from ≈ 0.87 to 0.95 (Anav et al., 2015), whereas it is 0.92 for SEDGES. The same correlations between the three models and CARBONES ranges from ≈ 0.83 to 0.87 (Anav et al., 2015), whereas it is 0.86 for SEDGES.

SEDGES simulates well the climatological annual cycles of GPP. Figure 3 shows monthly mean climatology of GPP for different latitudinal bands for SEDGES and the MTE dataset. From this figure, we can see that SEDGES captures well the seasonal progressions of GPP. A noticeable departure of SEDGES from MTE, however, is a slight phase shift in the northern hemisphere extratropics, with a generally earlier spring productivity increase in SEDGES than in MTE. We suspect that the phase shift is due to the absence of both winter-deciduous leaf phenology and physiological constraints on speed of acclimation to temperature (discussed more in appendix A). Moving to the full spatial field, Fig. 4 shows that the correlations in the seasonal cycle between SEDGES and MTE are generally high in areas with strong seasonality of productivity such as the mid to high latitudes, India, and the dry tropics. Temporal correlations are weaker, but still generally positive, in semi-arid regions and in Amazonia. Correlations are often negative in regions with low absolute seasonal variation in GPP such as equatorial Africa, the northern hemispheric deserts, and southern Australia. SEDGES' problems in the dry regions may be due to the simple single-layer bucket soil hydrology that was used. The negative correlation in equatorial Africa is due to insufficient moisture stress in that region in ERA-Interim-forced SEDGES. The lack of moisture stress in this region causes dry season GPP to exceed that of the wet season due to the reduced cloud cover, as is seen in the wetter parts of the Amazon (Wu et al., 2016). However, the real African equatorial forest experiences a drop in GPP during the dry season relative to wet season (Guan et al., 2015). Thus, the real world behavior in equatorial Africa is anti-correlated with that in the model. In equatorial Africa,

Geosci. Model Dev. Discuss., doi:10.5194/gmd-2017-75, 2017
Manuscript under review for journal Geosci. Model Dev.
Discussion started: 5 May 2017

Geoscientific Model Development Discussions

the lack of moisture stress in ERA-Interim-forced SEDGES is likely attributable to a pronounced positive precipitation bias in the ERA-Interim forcing data in that region (Lorenz and Kunstmann, 2012; Dolinar et al., 2016).

The interannual variability of global GPP for 1990-2009 in SEDGES is 1.79 $\mathrm{PgC\ yr^{-1}}$, whereas it is 2.50 $\mathrm{PgC\ yr^{-1}}$ for the CARBONES dataset. Anav et al. (2015) report values of 3.23, 4.4, and 2.87 $\mathrm{PgC\ yr^{-1}}$ for offline-driven land surface models, ORCHIDEE, JULES, and CLM4CN, respectively. The interannual variability of GPP at each grid point is shown in Fig. 5 for SEDGES and CARBONES. SEDGES successfully captures the spatial pattern of the CARBONES reference dataset, although its magnitudes are smaller, overall.

The trend in annual GPP for 1990-2009 is captured extremely well by SEDGES. The CARBONES reference dataset yields a global annual GPP trend of 0.086 $\mathrm{PgC\ yr^{-2}}$, whereas SEDGES gives a value of 0.080 $\mathrm{PgC\ yr^{-2}}$. The spatial pattern of the trend is seen in Fig. 6. SEDGES captures the spatial pattern of GPP trend in the CARBONES dataset better than ORCHIDEE, JULES, and CLM4CN, as reported by Anav et al. (2015). SEDGES generally outperforms the other models in Africa, Australia, the semi-arid areas of eastern Europe, and central and eastern Asia. Notable areas where SEDGES (but not the other models) deviates from CARBONES include Amazon and parts of northwestern North American, in which SEDGES simulates more negative trends in GPP than the reference dataset. The negative GPP trend in SEDGES in the Amazon is very possibly due, at least in part, to its simplifications affecting $\mathrm{CO_2}$ fertilization of productivity, as is explained next.

The SEDGES treatment of $\mathrm{CO_2}$ fertilization is seen via Eqs. (3) and (6) and notably lacks a direct dependency on temperature. However, Long (1991), using the widely-used Farquhar model of photosynthesis (Farquhar et al., 1980), finds that, for a given $\frac{c_i}{c_a}$, the proportional increase in leaf photosynthesis with elevated $\mathrm{CO_2}$ increases substantially with temperature under both Rubisco- and light-limited conditions. In line with that result, a modeling study at the scale of a global grid (Hickler et al., 2008) which uses a photosynthesis model based on that of the Farquhar one, finds the fertilization response of NPP to elevated $\mathrm{CO_2}$ increases substantially, too, when moving from boreal forest to temperate forest to tropical forest. Hence, if SEDGES were to use a more complex parameterization of photosynthesis that is based on the Farquhar model, one would expect the Amazon region to show a more positive GPP trend in Fig. 6 and thus be closer to the CARBONES data.

In spite of the simplifications affecting $\mathrm{CO_2}$ fertilization in SEDGES, its global productivity response to $\mathrm{CO_2}$ forcing is comparable to that of other models of the land surface and vegetation. The results of transient experiments in which 10 such models are forced offline with repeated early 20th century climate and with increasing $\mathrm{CO_2}$ values show relative increases of global NPP per $\mathrm{ppm\ CO_2}$ of 0.05% to 0.20% (with mean of 0.16%) for the 1980-2009 period (Piao et al., 2013); it is 0.102% for SEDGES. Similar transient simulations with 5 of the aforementioned models (but also including projected $\mathrm{CO_2}$ levels) (Sitch et al., 2008) give global GPP increases[8] from 280 to 360$\mathrm{ppm\ CO_2}$ that range from approximately 14% to 19%; they give global GPP increases from 360 to 560$\mathrm{ppm\ CO_2}$ that range from approximately 23% to 36%. In comparison, the transient run of SEDGES gives an increase in global GPP from 280 to 360$\mathrm{ppm\ CO_2}$ of 20%, and an at-equilibrium global GPP increase from 360 to 560$\mathrm{ppm\ CO_2}$ of 30%. Finally, Hemming et al. (2013), approximating the purely physiological

[8] visually estimated from their Fig. 9

Geosci. Model Dev. Discuss., doi:10.5194/gmd-2017-75, 2017
Manuscript under review for journal Geosci. Model Dev.
Discussion started: 5 May 2017

Geoscientific Model Development Discussions

effect[9] of CO_2 on productivity using a GCM, finds an increase in equilibrium GPP of 75% when doubling CO_2 from near-pre-industrial values. A most likely increase in global NPP of 40% to 60% with CO_2 doubling from pre-industrial levels is found by Holden et al. (2013), using a combination of global atmospheric CO_2 rise and estimated land use changes since the pre-industrial. Doubling pre-industrial CO_2 (280 to 560ppm) in equilibrium simulations in SEDGES induces an NPP increase of 55%.

5.2 Evaluation of Vegetative Carbon

Vegetative carbon is simulated reasonably well by SEDGES. Unless stated otherwise, we compare the means of the last 30 years of the CO_2-varying run with an older reference dataset (Olson et al., 1985). The Olson dataset was chosen because its data sources reflect the potential natural vegetation better than the sources of the more recent NDP-017b dataset (Gibbs, 2006). SEDGES has an equilibrium global vegetative carbon of 530PgC under pre-industrial levels of CO_2, and a mean of 615PgC for 1981-2010 of the transient CO_2 run. In comparison, the Olson et al. (1985) dataset and the more recent Gibbs (2006) dataset give a global vegetative carbon of 451PgC and 560PgC, respectively (Jiang et al. (2015), citing Gibbs (2006)).

The spatial pattern of Olson vegetative carbon is captured well by SEDGES (table 3: R = 0.57, R^2 = 0.33). This R^2 value compares favorably with the range of values (0.14 to 0.38) given by Jiang et al. (2015) for 11 Earth system models.

The RMSE (root mean squared error) between SEDGES and the Olson datasets is 3.92kgC m^{-2}, whereas it ranges from 3.01kgC m^{-2} to 7.18kgC m^{-2} for the models in Jiang et al. (2015).[10] More specifically, Fig. 7 shows the distributions of mean vegetative carbon for SEDGES (1981-2010) and that for the Olson et al. (1985) dataset. Two tendencies in the discrepancies prevail: the almost-direct relationship between GPP biases and vegetative carbon biases, and an overall tendency to overestimate vegetative carbon in the tropics and to underestimate it in the mid to high latitudes. SEDGES has large positive vegetative carbon biases in most of the tropics (except the western Amazon), southeast North America, China, and northwestern Europe. One should note that many of these biases reflect land cover change from forests to croplands (Ramankutty and Foley, 1999). In addition, positive biases in the wet-and-dry and semi-arid tropics are partially attributable to the absence of a fire module in SEDGES; fire can have a large impact on vegetative cover in these regions (Bond et al., 2005). SEDGES has large negative biases in western Canada and central Siberia. The subarctic is generally negatively-biased. These vegetative carbon biases are due to a combination of the aforementioned GPP biases and the globally-uniform residence time for vegetative carbon in SEDGES (table 1). The SEDGES 10 year residence time for vegetative carbon matches the observation-based estimate ($\equiv \frac{C_{veg}}{NPP}$) given by Jiang et al. (2015).

[9] In addition to the direct impact of CO_2 on GPP, some vegetation feedback onto GPP via climate is included here; also, vegetation distributions and LAI are held fixed.

[10] We calculate RMSE in this study by taking the square root of an area-weighted mean of the squared differences between SEDGES and the reference at each grid point. Jiang et al. (2015) uses the simple mean across all grid points.

Geosci. Model Dev. Discuss., doi:10.5194/gmd-2017-75, 2017
Manuscript under review for journal Geosci. Model Dev.
Discussion started: 5 May 2017

5.3 Evaluation of Soil Carbon

At present, land surface models have great difficulty in simulating soil carbon well. Tian et al. (2015), using 10 offline-forced terrestrial biosphere models, find highly diverging model estimates of soil organic carbon dynamics as well as systematic biases due to absent processes affecting high latitude soil carbon stocks. A study by Todd-Brown et al. (2013) finds RMSE's from ≈ 9 to $21 \mathrm{kgC\,m^{-2}}$ in a comparison of 16 Earth system models with the Harmonized World Soil Database (HWSD) reference dataset (Wieder et al., 2011) at 1° resolution. At the coarser T62 resolution and run offline, 3 SEDGES performs better with $7.9 \mathrm{kgC\,m^{-2}}$ RMSE. The models in both studies (Todd-Brown et al., 2013; Tian et al., 2015) have Pearson correlation coefficients under 0.4 with respect to the HWSD data, although model performance improves dramatically at coarser spatial scales (Todd-Brown et al., 2013). Again, SEDGES performs better with a 0.58 correlation.

Figure 8 shows the full spatial distribution of soil carbon for SEDGES and the HWSD reference dataset. Compared to HWSD, SEDGES simulates less soil carbon in semi-arid and arid areas, in the more northern parts of the Arctic, and generally more soil carbon in the remaining areas.

Taking the globe as a whole, SEDGES has a residence time for soil carbon of 25.7 years and a time-averaged soil carbon of $1516 \mathrm{PgC}$ for 1981-2010. Respective estimates for these values based on HWSD data are 24 years for residence time (Todd-Brown et al., 2013) and range from $891 \mathrm{PgC}$ to $1657 \mathrm{PgC}$ for total terrestrial soil carbon storage (Tian et al., 2015). Köchy et al. (2015) estimate total terrestrial soil carbon at a higher value of $\approx 3000 \mathrm{PgC}$ because they include estimates of carbon in the deeper soil layers that HWSD does not.

5.4 Evaluation of LAI

We use reprocessed Moderate Resolution Imaging Spectroradiometer (MODIS) data from 2001 to 2010 from Bejing Normal University (BNU) (Yuan et al., 2011) as the reference set. We interpolated this data to T62 resolution and derived a monthly mean climatology from it. Outside of the tropics, we compare only the maximum of the climatological monthly means of LAI between SEDGES and the reference data because of the absence of cold deciduous phenology in SEDGES and because serious deficiencies with MODIS in capturing the seasonal cycle of LAI in boreal coniferous forests have been found (Serbin et al., 2013).

Figure 9 shows maximum climatological LAI in SEDGES and the BNU MODIS-based reference, for the years, 2001 to 2010. SEDGES has strong positive biases in southeastern and extreme northern South America, in parts of Africa, in parts of southern and eastern Asia, in northern coastal Australia, and in parts of Europe. Many of these LAI biases lie where positive GPP biases occur and/or where croplands have replaced natural forests. Strong negative biases occur in parts of northern Asia. Of these, the biases east and northeast of Lake Baikal occur in the absence of negative GPP biases. Overall, the spatial patterns of maximum LAI in SEDGES and the MODIS-based reference have a correlation of 0.793.

Figure 10 shows the temporal correlation in the tropics between the monthly mean climatologies of SEDGES and the BNU MODIS-based reference (i.e. the correlations of the two season cycles). In spite of the crude scheme for drought-deciduous phenology described in section 2.2.8, SEDGES does a reasonable job in simulating the seasonal cycle of LAI in much of

Geosci. Model Dev. Discuss., doi:10.5194/gmd-2017-75, 2017
Manuscript under review for journal Geosci. Model Dev.
Discussion started: 5 May 2017

Geoscientific Model Development Discussions

the tropics. Negative correlations (indicative of poor model performance) occur near the equator, especially in the Amazon region, where LAI varies modestly, seasonally, in the real world (e.g., Wu et al., 2016). The wet parts of the Amazon generally experience high water availability, even in the dry season. As a result, LAI there is decoupled from soil moisture-induced water stress (in contrast with the drier portions of the Amazon), and LAI, generally, is increasing during the dry season and decreasing during the wet season (Wu et al., 2016). SEDGES cannot capture this behavior.

5.5 Evaluation of Surface Albedo

Figure 11 shows monthly mean climatologies of SEDGES surface albedo and MODIS white sky albedo (NASA LP DAAC, b)[11] for the months of January, April, July, and October for the years 2001 to 2010. From these figures, we can see that SEDGES captures the overall spatial albedo pattern fairly well. In fact, spatial correlations between SEDGES and the reference range from a low of 0.77 in July, and August to a high of 0.91 in April. The high correlation in boreal spring indicates relative strength in simulating the winter melt season at mid to high northern latitudes. The relative weakness of SEDGES in Northern Hemispheric summer is due to the absence of a strong snow signature on the land and relative weakness of the model in correctly capturing the second and third order determinants of (non-glacier) terrestrial albedo, since these determinants come to the fore during boreal summer. Three such determinants are now discussed.

The most significant model deficiency in albedo simulation that gains prominence during boreal summer is the simulation of bare soil surface albedos. Recall from section 2.3.1 that bare surface albedo in SEDGES is determined by soil carbon content and by the albedo of soil in the absence of soil carbon (α_{sand}), which is assumed constant. In the real world, geological processes, the quantity and properties of dead biomass litter, and the albedo of the underlying bedrock greatly impact α_{sand} as well (Knorr and Schnitzler, 2006; Vamborg et al., 2011). The absence of these real world processes in SEDGES gives rise to an underestimate of albedo in the Arabian and the Saharan deserts and an overestimate of albedo in the snow-free season in most of the world's remaining deserts (Fig. 11). MODIS values of snow-free albedo (NASA LP DAAC, a) in the polar desert (not shown) vary generally from 0.12 to 0.22 in July. The negative soil carbon bias in SEDGES in the high Arctic (section 5.3) causes the snow-free albedo to be too high in polar deserts of the high Arctic.

A second major model deficiency in boreal summer albedo simulation stems from SEDGES's inability to distinguish between low albedo (≈0.09) evergreen coniferous forests and high albedo (≈0.16) mid or high latitude broadleaf deciduous forests. This deficiency is seen most clearly in July (Fig. 11) in eastern North America, in which SEDGES fails to capture the south-to-north decrease in albedo from the temperate to subarctic regions.

The third significant model deficiency in the simulation of albedo during boreal summer is a negative bias in areas that are grassland or savanna in the real world, particularly those found in Mongolia, the U.S. Great Plains, and tropical Africa. In

[11] The original MODIS data were processed by spatially interpolating to fill in missing data, taking multi-year means (i.e. means across multiple years) of the 23 16-day periods for each year, spatially interpolating these into T62 resolution, temporally interpolating the 16-day periods linearly to obtain 24 new such periods such that each month was covered by two periods, taking the mean of the two periods for each month, masking out albedo values for each month and region that had polar night-caused missing values in its original pre-interpolated comprising data, and masking out water and land ice grid points in the ERA-Interim reanalysis T62 data that was used to forced SEDGES. White sky albedo from MODIS was used as the reference dataset because SEDGES's albedo formulation lacks dependency on the zenith angle of the direct beam.

Geosci. Model Dev. Discuss., doi:10.5194/gmd-2017-75, 2017
Manuscript under review for journal Geosci. Model Dev.
Discussion started: 5 May 2017

Geoscientific Model Development Discussions

the latter two regions, this negative albedo bias is associated with a positive bias in vegetative carbon (section 5.2) and LAI (Fig. 9).

Positive biases in vegetative carbon in the mid to high latitudes also cause a lowering of SEDGES January albedo as compared to MODIS (Fig. 11). The most affected regions are in central Asia and the North American prairies and High Plains.[12]

Finally, it must be noted that our albedo evaluations of SEDGES has been with respect to white sky albedo, and not actual albedo.

5.6 Evaluation of Evapotranspiration and Runoff

Evapotranspiration from SEDGES is compared to that of a multi-source compilation reference dataset, Mueller et al. (2013), for the period from 1989 to 2005. Simulated evapotranspiration by SEDGES qualitatively follows that of the reference dataset, successfully capturing the first order annual and seasonal zonal mean patterns (Fig. 12). Some salient deficiencies exist, however.

The most severe discrepancy is the excessive ET simulated by SEDGES in the mid- to high northern latitudes, which is most pronounced in the transition season from late winter to early spring (Fig. 12). This ET bias occurs because the new parameterization (see section 2.2.5) to reduce excessive sublimation from snow-covered surfaces in the original SimBA parameterization is only moderately effective. This deficiency is possibly the most crucial one to improve in future model versions. Another major contributor to the mid- to high northern latitude ET bias is the absence of winter-deciduous leaf phenology and the assumed instantaneous temperature acclimation in SEDGES (appendix A), which together increase spring GPP (section 5.1) and thus, concomitantly, increase transpiration.

In addition to the northern mid- to high latitude positive bias, SEDGES suffers from a negative ET bias in the equatorial region (Fig. 12), which has at least three likely causes. There is a negative bias in the incident surface shortwave radiation field in the ERA-Interim reanalysis data (Zhang et al., 2016) on the order of $\approx 5\%$ to 30% throughout most of the equatorial tropics for at least 6 months of the year. This bias may result in a relative reduction of GPP of similar magnitude, which would help to explain the negative GPP bias that SEDGES simulates here (seen in Figs. 1 and 2), while also explaining a reduction in transpiration of comparable (but lesser) magnitude. The latter would result from the increased canopy resistance (Eq. 12) that would ensue from the decreased demand for CO_2 uptake due to the lower light. The second reason for low ET near the equator is the complete absence of canopy interception loss in SEDGES, since this source of surface evaporation has been found to comprise around 20% of total ET in tropical rainforests (Shuttleworth, 1988; Da Rocha et al., 2004; Czikowsky and Fitzjarrald, 2009; Miralles et al., 2011)[13]. Finally, the low vapor pressure deficits in the wet tropics do not activate a mechanism in SEDGES that, in other models, would increase transpiration. Less transpiration is simulated by SEDGES in this region because SEDGES's simplifying assumption of a fixed $\frac{c_i}{c_a}$ promotes underestimation (overestimation) of transpiration

[12] Even though these areas would be mostly grasslands rather than cropland if not for human land cover change (Ramankutty and Foley, 1999), the winter albedo would be similarly high in either case.

[13] Here, we combine in-situ precipitation and ET data from Da Rocha et al. (2004) with a ground-observed interception loss-to-precipitation ratio of 0.116 from nearby (as reported by Czikowsky and Fitzjarrald, 2009) to get an interception loss-to-ET ratio of 0.22

Geosci. Model Dev. Discuss., doi:10.5194/gmd-2017-75, 2017
Manuscript under review for journal Geosci. Model Dev.
Discussion started: 5 May 2017

Geoscientific Model Development Discussions

when vapor pressure deficits are low (high), due to the increase of $\frac{c_i}{c_a}$ with decreasing vapor pressure deficit (Medlyn et al., 2011, 2012; Prentice et al., 2014). It then follows from Fick's law of diffusion (at the plant scale) that higher $\frac{c_i}{c_a}$ decreases the leaf-to-air CO_2 gradient, thus requiring that stomatal conductance increase to ensure sufficient CO_2 inflow for photosynthesis. The higher stomatal conductance increases transpiration. A similar process happens at the canopy scale.

Conspicuously high ET can be seen toward the end of the wet season in both the northern and southern edges of the tropics in Fig. 12. A very similar zonal mean temporal pattern is found in transpiration in the STEAM land surface model (Fig. 6 of Wang-Erlandsson et al., 2014). Because this model was evaluated using ERA-Interim forcing data, the high ET anomalies that we see in Fig. 12 may be attributable to this particular forcing; the ET anomalies in SEDGES may also be attributable to the lack of canopy interception loss, which declines in tandem with precipitation toward the end of the wet season in Wang-Erlandsson et al. (2014), thus reducing the magnitude of the ET aberrations.

The percentage of global evapotranspiration coming from transpiration is 64% in SEDGES, which compares very well with a literature-based estimate of 61% (with 15% standard deviation), derived from 81 studies (Schlesinger and Jasechko, 2014).

Simulated runoff is compared to the composite gridded dataset from the University of New Hampshire (UNH) and World Meteorological Organization's Global Runoff Data Centre (GRDC) (Fekete et al., 2002). SEDGES simulates runoff well except for excesses in the equatorial tropics and in the mid latitudes of the Southern Hemisphere (Fig. 13). Excessive runoff in the equatorial tropics is due to the aforementioned low ET, but it is also attributable to a general overestimate of precipitation in these latitudes by the ERA-Interim reanalysis (Lorenz and Kunstmann, 2012; Dolinar et al., 2016). Global runoff for SEDGES, excluding areas of land ice, is about 44 $\times 10^{15}$ kg yr^{-1}, which is slightly higher than the 38 $\times 10^{15}$ kg yr^{-1} for the UNH/GRDC dataset and the global (excluding Antarctica) runoff estimate of 37 $\times 10^{15}$ kg yr^{-1} by Dai and Trenberth (2002).

It should be noted that the parameterization for soil water holding capacity (section 2.3.2) gives generally much lower values (not shown) in the wet and dry tropics than in the reference dataset (Kleidon and Heimann, 1998; Hall et al., 2006; Kleidon, 2011). Such lower values of soil water holding capacity should lead one to expect a positive runoff bias in these areas in SEDGES. This is not the case, however, when we compare those regions of the wet and dry tropics where the ERA-Interim precipitation forcing has insignificant bias (and where biases in SEDGES runoff are thus unlikely to be attributable to precipitation deficiencies in the forcing). The lack of runoff bias in these regions suggests that the parameterization of soil water holding capacity in SEDGES (Eq. 26) works well in tandem with its ET scheme and the simple soil bucket hydrology (Eq. 29).

Finally, while it might seem easy to attribute deficiencies in the SEDGES hydrology to our use of the single layer soil bucket, this type of model has been found to perform well under many conditions: wet soils, when precipitation events tend to be large relative to the bucket depth, and under strong root compensation or hydraulic redistribution of soil moisture (Guswa et al., 2002; Guswa, 2005). Even when the aforementioned conditions do not hold, distortions stemming from use of the single layer bucket model are comparable to those coming from other aspects of SEDGES hydrology.

Geosci. Model Dev. Discuss., doi:10.5194/gmd-2017-75, 2017
Manuscript under review for journal Geosci. Model Dev.
Discussion started: 5 May 2017

5.7 Evaluation of Forest Cover Fraction

The overall global pattern of tree cover fraction of the International Satellite Land Surface Climatology Project (ISLSCP II) reference dataset (DeFries and Hansen, 2009) is captured reasonably well by SEDGES, as seen from Fig. 14. However, SEDGES has almost double the amount of arboreal cover. In Europe, China, and India, this is at least partially due to anthropogenic land cover change of natural forests and woodland to croplands (Ramankutty and Foley, 1999). Aside from this deforestation, the model's lack of competing plant functional types (especially boreal trees, warm region trees, and grasses) in conjunction with the constant residence time of 10 years for all vegetative carbon, leads to an overestimation of arboreal vegetation by SEDGES in South America, Africa, and North America, as well as a slight underestimation in boreal forest regions. A noted limitation of the reference dataset is its underestimation of real world tree cover in areas with the highest cover fraction. Thus, SEDGES' overestimates in these regions may partially be due to this phenomenon, as well. Finally, a less inclusive definition for arboreal cover in the reference dataset than in SEDGES contributes to the cover overestimate in the latter. SEDGES assumes that forest is vegetated land that protrudes above the winter snow pack, whereas the ISLSCP II dataset requires that trees be at least $5\mathrm{m}$ tall to count toward tree cover and thus excludes short trees and tall shrubs that do not get completely buried by snow.

5.8 Model Evaluation: Summary and Conclusions

The performance of the new SEDGES model has been evaluated for the present day through comparison with numerous reference land datasets. To do this, we have forced SEDGES offline with ERA-Interim reanalysis data, using our recommended simple single layer bucket soil hydrology to simulate terrestrial water storage, incorporating a simple scheme to handle a snow-temperature mismatch in the forcing data, and adopting the Planet Simulator's formulation for aerodynamic conductance. Note that the particular forcing data and hydrological implementations impact the analyzed output of the SEDGES simulations. In particular, the spin up using repeated climatology from 1981-2010 yields conditions that differ from a spin up using purely historical data. Not only do forcing and hydrology affect the model evaluation, but so do the reference datasets against which it is compared, since even they are not perfect representations of reality. Given all of these particularities, one must view the presented evaluation as a conditional, non-definitive, but yet informative guide to the strengths and the weakness of the model.

The following output variables of SEDGES have been examined: GPP, vegetative carbon, soil carbon, LAI, surface albedo, ET, runoff, and forest cover fraction. In comparison to the respective reference datasets, SEDGES simulates each variable at least reasonably well. Relative model strengths lie in the simulation of GPP; relative weaknesses in ET, snow-free albedo, and forest cover fraction. Given the simplicity of its formulation, the strength in GPP is unexpected, particularly the ability of SEDGES to capture the spatial patterns of temporal trends in GPP. Simulated ET is too high in the mid to high northern latitudes and is too low in the wet tropics. SEDGES captures albedo patterns fairly well outside of boreal summer, but subtler differences among the different desert types and among the non-desert areas are not well-captured during the snow-free season. Simulated forest cover fraction is generally too high.

Geosci. Model Dev. Discuss., doi:10.5194/gmd-2017-75, 2017
Manuscript under review for journal Geosci. Model Dev.
Discussion started: 5 May 2017

6 Discussion and Conclusions

A new simplified model for the representation of dynamic ecological processes for use in conjunction with climate models has been developed. This new model was forced with reanalysis data in order to compare the simulated present-day land surface with observational datasets. The quantitative comparison highlighted strengths and weaknesses of the model. A notable strength is that SEDGES's simulation of gross primary productivity is comparable to and sometimes better than that of state-of-the-art dynamic global vegetation models. Our evaluation has also shown that SEDGES performs well in a number of other metrics. Overall, the results show that SEDGES can be used to adequately simulate modern land surface characteristics, including input variables to land-atmosphere coupling schemes used in climate models, as well as key variables of the hydrological and terrestrial carbon cycles.

The most severe weaknesses of our offline-run SEDGES are the strong positive evapotranspiration bias that it yields in the mid-to-high latitudes in winter and early spring and its over-prediction of arboreal cover. The latter results from the use of only one plant functional type, which, along with a fixed relationship between biomass and both wet soil LAI and rooting depth hydrology, excessively constrains large scale vegetation structure by excluding the emergence of location-adapted landscape characteristics. As result of these issues, simulated vegetation in water-limited regions and wetness-induced changes should be treated as more heuristic than definitive. With respect to simulating terrestrial carbon pool changes, SEDGES's use of a single soil carbon reservoir and its fixed residence time for vegetative carbon may also need to be considered when drawing inferences from model results in transient simulations (e.g., see Friend et al., 2014).

For its level of complexity, SEDGES and the land surface framework which it presupposes have the advantages of a flexible time step, canopy control over transpiration, transpiration that is fully coupled to photosynthesis, and vegetative productivity that depends on light and not just temperature and moisture. The short time step option permits SEDGES to be incorporated into models that resolve the diurnal cycle. Because of these strengths, we expect SEDGES to have advantages over vegetation models of similar complexity in simulating vegetation, primary productivity, and transpiration in past geological warm periods in regions that receive little sunlight (e.g. the Eocene Arctic (Maxbauer et al. (2014) and references within)); and in simulating cloud-vegetation feedbacks in all eras. The SEDGES framework uses photosynthetic-driven stomatal control over evapotranspiration, which is critical when studying hydrological changes on land under altered atmospheric CO_2 concentrations, including anthropogenically-induced warming scenarios (Betts et al., 2007).

The SEDGES framework has the advantages of being easier to understand, process-wise, as compared to more complex vegetation and hydrological schemes. Increased vegetation model complexity can obfuscate model behavior, and it need not improve performance. In an intermodel comparison of the performance of 24 vegetation models at 39 eddy covariance flux tower sites, Schaefer et al. (2012) finds insignificant effects of sunlit-shaded leaf differentiation, nitrogen cycle inclusion, and having a light use efficiency or enzyme kinetic approach to productivity on a model's capacity to simulate GPP. Moreover, even when present-day biome distributions are well-simulated by complex vegetation models, model behaviors can diverge drastically from each other under non-present conditions due to differing physiological assumptions (e.g. climatic limitations

Geosci. Model Dev. Discuss., doi:10.5194/gmd-2017-75, 2017
Manuscript under review for journal Geosci. Model Dev.
Discussion started: 5 May 2017

within plant functional types) that are not well-grounded and that may very well change under novel climatic, atmospheric CO_2, and nutrient conditions (Fisher et al., 2015).

In conclusion, we feel that SEDGES provides a new viable and computationally efficient alternative to currently-implemented terrestrial vegetation/ecological models, in particular inside Earth System Models of Intermediate Complexity and for research on the global scale interactions between the physical climate system and the terrestrial biosphere.

7 Code availability

Both the SEDGES model code and the code we used to drive SEDGES with external data are available from the following digital repository:
https://zenodo.org/badge/latestdoi/88959747

8 Data availability

ERA-Interim reanalysis data (Dee et al., 2011) available from http://apps.ecmwf.int/datasets/data/interim-full-daily/. The atmospheric CO_2 data are available from $\mathrm{ftp://aftp.cmdl.noaa.gov/products/trends/co2/co2\_annmean\_mlo.txt}$ for Mauna Loa record and from http://cdiac.ornl.gov/ftp/trends/co2/lawdome.smoothed.yr20 for the ice core data. We used the $\mathrm{EnsembleGPP\_GL.nc}$ file of the MTE GPP dataset (Jung et al., 2011), which is available from https://www.bgc-jena.mpg.de/geodb/projects/Home.php. The CARBONES GPP dataset was obtained from http://www.carbones.eu/wcmqs/. The vegetative carbon dataset (Olson et al., 1985) is available from $\mathrm{http://cdiac.ornl.gov/epubs/ndp/ndp017/ndp017\_1985.html}$. The HWSD soil carbon dataset HWSD) reference dataset (Wieder et al., 2011) is available from https://daac.ornl.gov/SOILS/guides/HWSD.html. The LAI data (Yuan et al., 2011) is available from http://globalchange.bnu.edu.cn/research/lai/. The MODIS white sky albedo data (NASA LP DAAC, b) and MODIS snow-free albedo data (NASA LP DAAC, a) are available from https://reverb.echo.nasa.gov/reverb/. The reference ET dataset (Mueller et al., 2013) can, upon registration, be download from http://www.iac.ethz.ch/group/land-climate-dynamics/research/landflux-eval.html. The UNH/GRDC runoff dataset (Fekete et al., 2002) can be obtained from http://www.grdc.sr.unh.edu/html/Data/index.html. The ISLSCP II tree cover dataset (DeFries and Hansen, 2009) is available from $\mathrm{https://daac.ornl.gov/cgi-bin/dsviewer.pl?ds\_id=931}$. The rooting zone plant available soil water storage capacity dataset (Kleidon and Heimann, 1998; Hall et al., 2006; Kleidon, 2011) is available from the following URL: $\mathrm{https://daac.ornl.gov/cgi-bin/dsviewer.pl?ds\_id=1006}$. Accessing these last two datasets requires registering and signing in.

Geosci. Model Dev. Discuss., doi:10.5194/gmd-2017-75, 2017
Manuscript under review for journal Geosci. Model Dev.
Discussion started: 5 May 2017

Geoscientific Model Development Discussions
Open Access
EGU

Appendix A: Notes on the Temperature Limitation Function

In this section, we discuss the rationale behind our particular temperature limitation multiplier, $f_2(T_{sfc})$, on the light-limited rate of gross primary productivity (Eq. 2) in section 2.2.3.

$f_2(T_{sfc})$ increases linearly from 0 at T_{sfc} of 0 °C to 1 at T_{sfc} of 20 °C and then plateaus at 1. The linear increase is chosen for its simplicity and because it is analogous to the often-used "growing degree days" (GDD) metric (with 0 °C base) in agriculture and ecology (Kauppi and Posch, 1985; Prentice et al., 1992; Kaplan, 2001) (save for the shorter time scale). SEDGES' critical temperature of 20 °C at which productivity is no longer limited lies close to the middle of the range of optimum temperatures for C3 plants (5 °C to 39 °C) that was found in a survey of 212 temperature response curves of photosynthesis in the literature for different species and growth temperatures (Way and Yamori, 2014; Yamori et al., 2014).

Temperature limitation on photosynthesis has been well studied (e.g., see reviews by Sage and Kubien, 2007; Yamori et al., 2014), but many uncertainties remain. In land plants, photosynthesis is significantly limited by both high and low temperatures. Individual plants of different species and from different environments have differing optimal temperatures for photosynthesis, such that away from the optimal temperature, photosynthetic rate decreases (Yamori et al., 2014). Around the temperature optimum, there exists a range of temperatures for which photosynthesis is nearly as high as at the optimum (Berry and Bjorkman, 1980; Yamori et al., 2014). Both the temperature dependency and the maximum rate of photosynthesis (realized at the temperature optimum) can shift as a plant acclimates to a different set of environmental conditions (Berry and Bjorkman, 1980; Way and Yamori, 2014; Yamori et al., 2014).

In most plants, temperature limitation on photosynthesis depends on the species, current light levels, the environmental conditions under which the plant grew, and the internal levels of CO_2 in the leaves (Berry and Bjorkman, 1980; Sage and Kubien, 2007; Way and Yamori, 2014; Yamori et al., 2014). In addition, the current temperature limitation depends on the extent of acclimation to recent environmental conditions (e.g., Dietze, 2014)

The framework in which we use $f_2(T_{sfc})$ assumes perfect acclimation and adaptation of the vegetation to the current weather and light conditions. As such, the SEDGES temperature limitation assumes the presence of the most productive set of plants that could ideally grow under those conditions and also by allowing for their instantaneous adaptation and acclimation to those conditions. In other words, for a given surface temperature (T_{sfc}), $f_2(T_{sfc})$ represents the universal physiological constraints on productivity exerted by that (isolated) given temperature.

For high temperatures, a conscious decision was made to not include a decline in productivity in SEDGES. Although it is well-established that high temperatures (i.e. temperatures above the optimum) limit productivity for individual plants, some of that limitation that has been found empirically may have been due to an indirect effect of temperature on increasing leaf-to-air vapor pressure deficit (for constant ambient relative humidity), which causes optimum temperature to be lower than when vapor pressure deficit is held fixed (Lin et al., 2012). An even more important point is that high temperature limitation reflects more the inability of plants that are adapted to a given environment to perform equally well under all conditions that they might face in that environment and less an intrinsic barrier for plant life at that location to adapt to a given high temperature regime (via some combination of species migrations, natural selection, evolution, and/or acclimation). For example, although the Yamori

Geosci. Model Dev. Discuss., doi:10.5194/gmd-2017-75, 2017
Manuscript under review for journal Geosci. Model Dev.
Discussion started: 5 May 2017

Geoscientific Model Development Discussions

et al. (2014) study found C3 plants to generally have temperature optima between 10 °C and 35 °C, light-saturated and CO_2-saturated photosynthesis for the C3 hot desert plant, *Rhazya stricta* shows no significant decline with leaf temperature even up to 44 °C (Lawson et al., 2014). Moreover, its (ordinary) daily photosynthetic rates are nearly as high as those of common C3 agricultural crops, in spite of living under natural conditions of much higher vapor pressure deficit and presumably much drier soil (Lawson et al., 2014), which reduce productivity. Similar results as for *Rhazya stricta* have been found for the C3 desert shrub, *Larrea divaricata* (Mooney et al., 1978). Thus, the large scale ability of vascular plant life to adapt to high temperatures through the increased prevalence of heat-tolerant species and phenotypes should be properly accounted for when modeling vegetation and the carbon cycle in past warm climates (such as the Cretaceous) as well as in future climates.

Appendix B: Numerical parameterization of canopy resistance and maximum transpiration rate

Canopy resistance is the greater of an unconstrained canopy resistance (r_{cu}), which is determined by the light-limited rate of canopy photosynthesis (GPP_L), and a canopy resistance set by the maximum rate at which the rooting zone can supply water for transpiration. The equation for the unconstrained canopy resistance is essentially derived by incorporating the canopy resistance (r_c) value from the previous time step, using the mismatch between GPP_W and GPP_L in the last time step, and accounting for updates to the variables that affect GPP_W and GPP_L. Although this formulation of r_{cu} depends on values from the previous time step, this dependency is arbitrary. An expression for r_{cu} that depends only on values in the current time step could be derived and used. (Such a r_{cu} would depend on all the variables that comprise GPP_W and GPP_L, and these variables would be evaluated at the current time step.)

Our starting equation for deriving the unconstrained canopy resistance uses the formulations of GPP_L and GPP_W given in Eqs. (2) and (6) and is as follows:

$$\begin{aligned} 0 &\equiv GPP_{L\,t+1} - GPP_{W\,t+1} \\ &\approx GPP_L \frac{f_{veg}}{f_{veg_{t-1}}} \frac{f_2(T_{sfc})}{f_2(T_{sfc_{t-1}})} \frac{SW{\downarrow}}{SW{\downarrow}_{t-1}} - GPP_W \frac{f_{veg}}{f_{veg_{t-1}}} \frac{1.6r_{ct-1} + r_{at-1}}{1.6r_{cu} + r_a}. \end{aligned} \tag{B1}$$

Here, the equivalence statement reflects the first stomatal goal of parsimoniously meeting the light-driven demand for CO_2. The future values of GPP_W and GPP_L are approximated (for simplicity) by neglecting changes in slowly varying variables (e.g., ρ). Equation (B1) represents the standard case for deriving r_c. Special cases are discussed below (e.g. when $f_{veg_{t-1}}$, $f_2(T_{sfc_{t-1}})$, or $SW{\downarrow}_{t-1}$ are zero.) Solving Eq. (B1) for r_{cu} yields

$$r_{cu} = \left(\frac{GPP_W}{GPP_L} \frac{f_2(T_{sfc_{t-1}})}{f_2(T_{sfc})} \frac{SW{\downarrow}_{t-1}}{SW{\downarrow}} (1.6r_{ct-1} + r_{at-1}) - r_a \right) \Big/ 1.6. \tag{B2}$$

Equation (B2) has provided us with r_{cu}, the canopy resistance that would occur in the complete absence of physiological limitations on plant water loss. In the real world, plants must restrict how much their stomata open when water cannot be extracted from the soil (or from internal plant storage) and transported to the leaf stomata fast enough to balance the loss

Geosci. Model Dev. Discuss., doi:10.5194/gmd-2017-75, 2017
Manuscript under review for journal Geosci. Model Dev.
Discussion started: 5 May 2017

Geoscientific Model Development Discussions
Open Access
EGU

to the atmosphere through the stomata. Doing so helps to keep water potentials within the plant from falling to levels that would cause "runaway" cavitation (Tyree and Sperry, 1988) or "hydraulic failure" (McDowell et al., 2008). Closing stomata increases stomatal resistances across the leaves, which, at the canopy scale, increases the canopy resistance. In this way, canopy resistance can be constrained by the supply rate of water from the soil to the leaves.

To simulate the maximum supply rate of water for transpiration, SEDGES adapts the simple model of Federer (1982). The original Federer maximum supply rate is directly proportional to the soil wetness fraction multiplied by a fixed constant parameter. This parameter is the *absolute* maximum transpiration value, which we denote here by "$trmax$". In SEDGES, we extend the original Federer formulation from the limited case of a fully-vegetated surface to the case of a mixed surface comprised of green leaves and exposed soil. This is achieved by simply multiplying the original expression by the vegetative cover fraction, f_{veg}. Thus, the supply rate for transpiration, S_{tr}, is as follows in SEDGES:

$$S_{tr} = f_{veg} \cdot \beta_{tr} \cdot trmax, \tag{B3}$$

where

β_{tr} is a water stress factor that affects the roots' ability to supply water for transpiration and equals the soil wetness fraction, W_{frac}, and

$trmax$ has a value of 2.78×10^{-7} m s^{-1}, which is taken from the BETHY vegetation model (Knorr, 2000). This maximum transpiration value is achieved only for a fully vegetated ($f_{veg} = 1$), fully wet soil.

The above extension of the original Federer formulation for water supply rate requires some justification. A reader that is familiar with the LPJ model might notice that SEDGES uses the same formulation as LPJ (Gerten et al., 2004); that is, both models multiply the original simple Federer expression ($S_{tr} = \beta_{tr} \cdot trmax$) by f_{veg} (on the right hand side). It is, however, inappropriate to simply borrow the LPJ formulation and apply it in SEDGES because the definitions of f_{veg} differ in the two models. In LPJ, the vegetative cover fraction is (approximately) the portion of a grid cell in which vegetation resides. Although this portion appears to change some with daily phenology (Gerten et al., 2004), the basic idea in LPJ seems to be that the vegetated portion of the grid cell is (essentially) completely vegetated, i.e. having roots, stems, and leaves. As such, it makes sense in LPJ to multiply the original Federer supply rate formulation by f_{veg} because this is the fraction of the grid cell that functions as in the Federer model. In contrast, SEDGES assumes that vegetation resides in the entire grid cell. In other words, SEDGES assumes that vegetation is spread throughout the grid cell uniformly, which means that plant roots and above-ground parts are also distributed uniformly at the large scale. Thus, in SEDGES, f_{veg} is created by the covering of bare soil by green leaves when looking down from above the canopy. As such, it is not obvious why the simple supply rate formulation in Federer (1982) is multiplied by f_{veg} in SEDGES. The answer lies in a close examination of the $trmax$ parameter of the original model.

The aforementioned simple supply rate model of Federer (1982) is tested, evaluated, and calibrated in the same paper against a more sophisticated "Type I" (Guswa et al., 2002) water uptake model that is forced using site-specific atmospheric observational data. Doing so reveals that the maximum transpiration rate (i.e. the $trmax$ parameter) in the simple model depends on the following input parameters for the Type I model (in decreasing order of strength): rooting density, root internal

Geosci. Model Dev. Discuss., doi:10.5194/gmd-2017-75, 2017
Manuscript under review for journal Geosci. Model Dev.
Discussion started: 5 May 2017

Geoscientific Model Development Discussions

resistance, depth of the rooting zone, and vegetation height/surface roughness. Although the first three of these dependencies are found to be substantial, those dependencies are not included in the simple model, which takes the $trmax$ parameter to be a constant. In addition, even the more sophisticated Type I water uptake model neglects soil drying-induced embolism's increase of root xylem resistance (e.g., Linton et al., 1998; Domec et al., 2004), which some authors (Domec et al., 2009; Javaux et al., 2013) feel plays a very significant or even dominant role in the whole plant conductivity of water. Significant increase in rooting zone xylem resistance decreases the maximum transpiration rate within the framework of the Type I model given in Federer (1982).

The missing dependencies in the original simple Federer formulation for maximum supply rate of transpiration presented in the last paragraph are addressed (though somewhat crudely) in SEDGES by multiplying the original formulation by the vegetative cover fraction, f_{veg}. Here, multiplication by f_{veg} becomes a proxy for the effect of decreasing root embolism with increasing soil wetness fraction in dry soils because f_{veg} increases with soil wetness fraction for very low values of soil wetness fraction (see Eq. 18). At low biomass values (≤ 0.25 kgC m^{-2}), f_{veg} is a proxy for rooting density because f_{veg} scales with biomass (through Eqs. 5 and 16) and so does rooting density (implicitly). At higher biomass values (> 0.25 kgC m^{-2}), f_{veg} serves as a proxy for rooting depth since both scale with biomass.

The water supply rate in the preceding discussion, as noted above, directly impacts the minimum canopy resistance, for which we will now derive an expression. Starting from Eqs. (12) and (7), it follows that

$$\frac{T}{ET} = \frac{f_{veg}}{(1 + r_c g_a) C_w}. \tag{B4}$$

Starting from Eq. (B4), we define $r_c min$ as the value of canopy resistance that matches the supply rate of transpiration in the current time step. That is, we have

$$f_{veg} \cdot \beta_{tr} \cdot trmax \equiv \frac{f_{veg}}{1 + r_c min\ g_a} \frac{ET}{C_w}, \tag{B5}$$

where we note that $\frac{ET}{C_w}$ is the potential evapotranspiration (PET) and $g_a = \frac{1}{r_a}$. Solving Eq. (B5) for $r_c min$ yields

$$r_c min = \left(\frac{PET}{\beta_{tr} \cdot trmax} - 1 \right) r_a. \tag{B6}$$

The final canopy resistance is restricted as follows:

$$r_c = min(r_c max, max(r_c min, r_{cu}, r_c min_{min})), \tag{B7}$$

where

$r_c min_{min}$ is the absolute minimum possible value for r_c and is set to 0 for simplicity, and

$r_c max$ is the maximum possible value for r_c and is set to an extremely large value, purely for the sake of model simplicity and elegance.

Geosci. Model Dev. Discuss., doi:10.5194/gmd-2017-75, 2017
Manuscript under review for journal Geosci. Model Dev.
Discussion started: 5 May 2017

Geoscientific Model Development Discussions

In deriving above Eqs. (B2), (B5), and (B6), we have excluded all cases in which we would have had to divide by variables with a zero value. These cases are handled as follows: Firstly, SEDGES checks to see if the light limited rate of GPP is zero in the next time step or if the soil is completely dry. If so, then canopy resistance is set to the maximum possible value. In the former case, there is no carbon benefit to keeping stomata open, and in the latter case, the supply rate is zero. If, however, the first check comes back negative for both conditions, then SEDGES checks for the case of parched soil getting rewetted. If this is the case, canopy resistance is set to the minimum value, r_cmin. If, however, the second check also comes back negative, then a final check is made to see if the light-limited rate of GPP is zero in the current time step. Under this last scenario, either the sun has risen or the surface temperature has risen above freezing in between the last and current time steps. Here, an expression for r_{cu} can be derived by substituting into Eq. (B1) a time-specifying version of Eq. (2): $GPP_{Lt+1} = \epsilon_{max} \cdot f_1(CO_2) \cdot f_2(T_{sfc}) \cdot f_{veg} \cdot SW\downarrow$. We then solve for the unconstrained canopy resistance and get the following:

$$r_{cu}* = \left(\frac{GPP_W}{\epsilon_{max} \cdot f_1(CO_2) \cdot f_2(T_{sfc}) \cdot f_{veg_{t-1}} \cdot SW\downarrow} (1.6 r_{ct-1} + r_{at-1}) - r_a \right) \Big/ 1.6. \tag{B8}$$

where the "*" is used to denote our special case of $GPP_{Lt+1} > 0$, $GPP_L = 0$, $W_{soil} > 0$, and $f_{veg_{t-1}} > 0$. After its computation in Eq. (B8), $r_{cu}*$ is restricted the same as r_{cu} is in Eq. (B7). In the case that the first, second, and final checks are all negative, then we have the standard scenario described by Eqs. (B2), (B5), and (B6).

Competing interests. The authors declare that they have no conflict of interest.

Acknowledgements. Climate Data Operators (CDO) was obtained from http://www.mpimet.mpg.de/cdo and was used to process much of the data. Version 6.2.1 of NCL (NCAR Command Language) was used to generate the plots (https://doi.org/10.5065/D6WD3XH5). Pablo Paiewonsky thanks Daniela Dalmonech for alerting us to severe deficiencies in the simulated evapotranspiration in an early version of SEDGES that ultimately led us to revise and much improve the model. Pablo Paiewonsky's work on the model's development was financially supported, in part, by the NSF-funded Alliance for Graduate Education and Professoriate (AGEP) program and by a Carson Carr Graduate Diversity Fellowship from the Office of Diversity, Equity, and Inclusion of the State University of New York.

Geosci. Model Dev. Discuss., doi:10.5194/gmd-2017-75, 2017
Manuscript under review for journal Geosci. Model Dev.
Discussion started: 5 May 2017

References

Amthor, J. S. and Baldocchi, D. D.: Terrestrial higher plant respiration and net primary production, Terrestrial global productivity, pp. 33–59, 2001.

Anav, A., Friedlingstein, P., Beer, C., Ciais, P., Harper, A., Jones, C., Murray-Tortarolo, G., Papale, D., Parazoo, N. C., Peylin, P., Piao, S., Sitch, S., Viovy, N., Wiltshire, A., and Zhao, M.: Spatiotemporal patterns of terrestrial gross primary production: A review, Reviews of Geophysics, 53, 785–818, 2015.

Beljaars, A., Brown, A. R., and Wood, N.: A new parametrization of turbulent orographic form drag, Quarterly Journal of the Royal Meteorological Society, 130, 1327–1347, 2004.

Berry, J. and Bjorkman, O.: Photosynthetic response and adaptation to temperature in higher plants, Annual Review of Plant Physiology, 31, 491–543, 1980.

Best, M., Pryor, M., Clark, D., Rooney, G., Essery, R., Ménard, C., Edwards, J., Hendry, M., Porson, A., Gedney, N., et al.: The Joint UK Land Environment Simulator (JULES), model description–Part 1: energy and water fluxes, Geoscientific Model Development, 4, 677–699, 2011.

Betts, A. K. and Ball, J. H.: Albedo over the boreal forest, Journal of Geophysical Research: Atmospheres, 102, 28 901–28 909, 1997.

Betts, R. A., Boucher, O., Collins, M., Cox, P. M., Falloon, P. D., Gedney, N., Hemming, D. L., Huntingford, C., Jones, C. D., Sexton, D. M., and Webb, M. J.: Projected increase in continental runoff due to plant responses to increasing carbon dioxide, Nature, 448, 1037–1041, 2007.

Blyth, E.: Estimating potential evaporation over a hill, Boundary-Layer Meteorology, 92, 185–193, 1999.

Bond, W. J., Woodward, F. I., and Midgley, G. F.: The global distribution of ecosystems in a world without fire, New phytologist, 165, 525–538, 2005.

Bowring, S., Miller, L., Ganzeveld, L., and Kleidon, A.: Applying the concept of ?energy return on investment? to desert greening of the Sahara/Sahel using a global climate model, Earth System Dynamics, 5, 43–53, 2014.

Brovkin, V., Ganopolski, A., and Svirezhev, Y.: A continuous climate-vegetation classification for use in climate-biosphere studies, Ecological Modelling, 101, 251–261, 1997.

Brovkin, V., Bendtsen, J., Claussen, M., Ganopolski, A., Kubatzki, C., Petoukhov, V., and Andreev, A.: Carbon cycle, vegetation, and climate dynamics in the Holocene: Experiments with the CLIMBER-2 model, Global Biogeochemical Cycles, 16, 1139, 2002.

Buckley, T. N. and Schymanski, S. J.: Stomatal optimisation in relation to atmospheric CO2, New Phytologist, 201, 372–377, 2014.

Campbell, G. and Norman, J.: An introduction to environmental biophysics., Ed. 2, Springer Science+Business Media Inc., New York, NY, USA, 1998.

Chen, F., Janjić, Z., and Mitchell, K.: Impact of atmospheric surface-layer parameterizations in the new land-surface scheme of the NCEP mesoscale Eta model, Boundary-Layer Meteorology, 85, 391–421, 1997.

Chen, Y., Yang, K., Zhou, D., Qin, J., and Guo, X.: Improving the Noah land surface model in arid regions with an appropriate parameterization of the thermal roughness length, Journal of Hydrometeorology, 11, 995–1006, 2010.

Cowan, I. and Farquhar, G.: Stomatal function in relation to leaf metabolism and environment, in: Symposia of the Society for Experimental Biology, edited by Jennings, D., 3, pp. 471–505, Cambridge University Press, Cambridge, UK, 1977.

Cox, P., Betts, R., Bunton, C., Essery, R., Rowntree, P., and Smith, J.: The impact of new land surface physics on the GCM simulation of climate and climate sensitivity, Climate Dynamics, 15, 183–203, 1999.

Cramer, W., Kicklighter, D., Bondeau, A., III, B. M., Churkina, G., Nemry, B., Ruimy, A., Schloss, A., and the participants of the Potsdam NPP model intercomparison: Comparing global models of terrestrial net primary productivity (NPP): overview and key results, Global change biology, 5, 1–15, 1999.

Czikowsky, M. J. and Fitzjarrald, D. R.: Detecting rainfall interception in an Amazonian rain forest with eddy flux measurements, Journal of hydrology, 377, 92–105, 2009.

Da Rocha, H. R., Goulden, M. L., Miller, S. D., Menton, M. C., Pinto, L. D., de Freitas, H. C., and Silva Figueira, A. M.: Seasonality of water and heat fluxes over a tropical forest in eastern Amazonia, Ecological applications, 14, s22–s32, 2004.

Dai, A. and Trenberth, K. E.: Estimates of freshwater discharge from continents: Latitudinal and seasonal variations, Journal of hydrometeorology, 3, 660–687, 2002.

Dee, D. P., Uppala, S. M., Simmons, A. J., Berrisford, P., Poli, P., Kobayashi, S., Andrae, U., Balmaseda, M. A., Balsamo, G., Bauer, P., Bechtold, P., Beljaars, A. C. M., van de Berg, L., Bidlot, J., Bormann, N., Delsol, C., Dragani, R., Fuentes, M., Geer, A. J., Haimberger, L., Healy, S. B., Hersbach, H., Hólm, E. V., Isaksen, L., Kållberg, P., Köhler, M., Matricardi, M., McNally, A. P., Monge-Sanz, B. M., Morcrette, J.-J., Park, B.-K., Peubey, C., de Rosnay, P., Tavolato, C., Thépaut, J.-N., and Vitart, F.: The ERA-Interim reanalysis: configuration and performance of the data assimilation system, Quarterly Journal of the Royal Meteorological Society, 137, 553–597, doi:10.1002/qj.828, http://dx.doi.org/10.1002/qj.828, 2011.

DeFries, R. and Hansen, M.: ISLSCP II Continuous Fields of Vegetation Cover, 1992-1993, http://daac.ornl.gov/ from Oak Ridge National Laboratory Distributed Active Archive Center, Oak Ridge, Tennessee, U.S.A., doi:10.3334/ORNLDAAC/931, accessed: 2016-02, 2009.

Dekker, S., De Boer, H., Brovkin, V., Fraedrich, K., Wassen, M., and Rietkerk, M.: Biogeophysical feedbacks trigger shifts in the modelled vegetation-atmosphere system at multiple scales, Biogeosciences, 7, 1237–1245, 2010.

DeLucia, E., Drake, J. E., Thomas, R. B., and Gonzalez-Meler, M.: Forest carbon use efficiency: is respiration a constant fraction of gross primary production?, Global Change Biology, 13, 1157–1167, 2007.

Desborough, C.: Surface energy balance complexity in GCM land surface models, Climate Dynamics, 15, 389–403, 1999.

Dewar, R. C.: A simple model of light and water use evaluated for Pinus radiata, Tree Physiology, 17, 259–265, 1997.

Dietze, M. C.: Gaps in knowledge and data driving uncertainty in models of photosynthesis, Photosynthesis research, 119, 3–14, 2014.

Dolinar, E. K., Dong, X., and Xi, B.: Evaluation and intercomparison of clouds, precipitation, and radiation budgets in recent reanalyses using satellite-surface observations, Climate Dynamics, 46, 2123–2144, 2016.

Domec, J.-C., Warren, J., Meinzer, F., Brooks, J., and Coulombe, R.: Native root xylem embolism and stomatal closure in stands of Douglas-fir and ponderosa pine: mitigation by hydraulic redistribution, Oecologia, 141, 7–16, 2004.

Domec, J.-C., Noormets, A., King, J. S., Sun, G., McNulty, S. G., Gavazzi, M. J., Boggs, J. L., and Treasure, E. A.: Decoupling the influence of leaf and root hydraulic conductances on stomatal conductance and its sensitivity to vapour pressure deficit as soil dries in a drained loblolly pine plantation, Plant, Cell & Environment, 32, 980–991, 2009.

Dutra, E., Balsamo, G., Viterbo, P., Miranda, P. M., Beljaars, A., Schär, C., and Elder, K.: An improved snow scheme for the ECMWF land surface model: description and offline validation, Journal of Hydrometeorology, 11, 899–916, 2010.

Dutra, E., Kotlarski, S., Viterbo, P., Balsamo, G., Miranda, P., Schär, C., Bissolli, P., and Jonas, T.: Snow cover sensitivity to horizontal resolution, parameterizations, and atmospheric forcing in a land surface model, Journal of Geophysical Research: Atmospheres, 116, 2011.

Essery, R.: Boreal forests and snow in climate models, Hydrological processes, 12, 1561–1567, 1998.

Etheridge, D., Steele, L., Langenfelds, R., Francey, R., Barnola, J.-M., and Morgan, V.: Historical CO2 records from the Law Dome DE08, DE08-2, and DSS ice cores, http://cdiac.ornl.gov/trends/co2/lawdome.html from Carbon Dioxide Information Analysis Center, Oak Ridge National Laboratory, U.S. Department of Energy, Oak Ridge, Tenn., U.S.A., in Trends: A Compendium of Data on Global Change., 1998.

Farquhar, G., von Caemmerer, S., and Berry, J.: A Biochemical Model of Photosynthetic CO2 Assimilation in Leaves of C3 Species, Planta, 149, 78–90, 1980.

Federer, C. A.: Transpirational supply and demand: plant, soil, and atmospheric effects evaluated by simulation, Water Resources Research, 18, 355–362, 1982.

Fekete, B. M., Vörösmarty, C. J., and Grabs, W.: High-resolution fields of global runoff combining observed river discharge and simulated water balances, Global Biogeochemical Cycles, 16, 2002.

Fisher, R., Muszala, S., Verteinstein, M., Lawrence, P., Xu, C., McDowell, N., Knox, R., Koven, C., Holm, J., Rogers, B., et al.: Taking off the training wheels: the properties of a dynamic vegetation model without climate envelopes, CLM4. 5 (ED), Geoscientific Model Development, 8, 3593–3619, 2015.

Franks, P. J., Adams, M. A., Amthor, J. S., Barbour, M. M., Berry, J. A., Ellsworth, D. S., Farquhar, G. D., Ghannoum, O., Lloyd, J., McDowell, N., Norby, R. J., Tissue, D. T., and von Caemmerer, S.: Sensitivity of plants to changing atmospheric CO2 concentration: from the geological past to the next century, New Phytologist, 197, 1077–1094, 2013.

Friend, A. D., Lucht, W., Rademacher, T. T., Keribin, R., Betts, R., Cadule, P., Ciais, P., Clark, D. B., Dankers, R., Falloon, P. D., et al.: Carbon residence time dominates uncertainty in terrestrial vegetation responses to future climate and atmospheric CO2, Proceedings of the National Academy of Sciences, 111, 3280–3285, 2014.

Gerten, D., Schaphoff, S., Haberlandt, U., Lucht, W., and Sitch, S.: Terrestrial vegetation and water balance?hydrological evaluation of a dynamic global vegetation model, Journal of Hydrology, 286, 249–270, 2004.

Gibbs, H.: Olson?s major world ecosystem complexes ranked by carbon in live vegetation: An updated database using the GLC2000 land cover product (NDP-017b)., http://cdiac.ornl.gov/epubs/ndp/ndp017/ndp017b.html from Carbon Dioxide Information Center, Oak Ridge National Laboratory, Oak Ridge, Tennessee, U.S.A., doi:10.3334/CDIAC/lue.ndp017.2006, 2006.

Gifford, R. M.: Plant respiration in productivity models: conceptualisation, representation and issues for global terrestrial carbon-cycle research, Functional Plant Biology, 30, 171–186, 2003.

Giorgi, F. and Avissar, R.: Representation of heterogeneity effects in earth system modeling: Experience from land surface modeling, Reviews of Geophysics, 35, 413–437, 1997.

Gower, S. T., Kucharik, C. J., and Norman, J. M.: Direct and indirect estimation of leaf area index, fAPAR, and net primary production of terrestrial ecosystems, Remote Sensing of Environment, 70, 29–51, 1999.

Guan, K., Pan, M., Li, H., Wolf, A., Wu, J., Medvigy, D., Caylor, K. K., Sheffield, J., Wood, E. F., Malhi, Y., et al.: Photosynthetic seasonality of global tropical forests constrained by hydroclimate, Nature Geoscience, 8, 284–289, 2015.

Guswa, A.: Soil-moisture limits on plant uptake: An upscaled relationship for water-limited ecosystems, Advances in water resources, 28, 543–552, 2005.

Guswa, A. J., Celia, M., and Rodriguez-Iturbe, I.: Models of soil moisture dynamics in ecohydrology: A comparative study, Water Resources Research, 38, 2002.

Hagemann, S.: An improved land surface parameter dataset for global and regional climate models, Tech. Rep. 336, Max-Planck-Institut für Meteorologie, http://www.mpimet.mpg.de/fileadmin/publikationen/Reports/max_scirep_336.pdf, 2002.

Hall, F. G., Brown de Colstoun, E., Collatz, G. J., Landis, D., Dirmeyer, P., Betts, A., Huffman, G. J., Bounoua, L., and Meeson, B.: ISLSCP Initiative II global data sets: Surface boundary conditions and atmospheric forcings for land-atmosphere studies, Journal of Geophysical Research: Atmospheres (1984–2012), 111, 2006.

He, L., Chen, J. M., Pisek, J., Schaaf, C. B., and Strahler, A. H.: Global clumping index map derived from the MODIS BRDF product, Remote Sensing of Environment, 119, 118–130, 2012.

Hemming, D., Betts, R., and Collins, M.: Sensitivity and uncertainty of modelled terrestrial net primary productivity to doubled CO2 and associated climate change for a relatively large perturbed physics ensemble, Agricultural and Forest Meteorology, 170, 79–88, 2013.

Heskel, M. A., Bitterman, D., Atkin, O. K., Turnbull, M. H., and Griffin, K. L.: Seasonality of foliar respiration in two dominant plant species from the Arctic tundra: response to long-term warming and short-term temperature variability, Functional Plant Biology, 41, 287–300, 2014.

Hickler, T., Smith, B., Prentice, I. C., Mjöfors, K., Miller, P., Arneth, A., and Sykes, M. T.: CO2 fertilization in temperate FACE experiments not representative of boreal and tropical forests, Global Change Biology, 14, 1531–1542, 2008.

Hikosaka, K. and Hirose, T.: Leaf angle as a strategy for light competition: optimal and evolutionarily stable light-extinction coefficient within a leaf canopy, Ecoscience, 4, 501–507, 1997.

Holden, P., Edwards, N., Gerten, D., and Schaphoff, S.: A model-based constraint on CO2 fertilisation, Biogeosciences, 10, 339–355, 2013.

Houldcroft, C. J., Grey, W. M., Barnsley, M., Taylor, C. M., Los, S. O., and North, P. R.: New vegetation albedo parameters and global fields of soil background albedo derived from MODIS for use in a climate model, Journal of Hydrometeorology, 10, 183–198, 2009.

Huntingford, C., Blyth, E., Wood, N., Hewer, F., and Grant, A.: The effect of orography on evaporation, Boundary-Layer Meteorology, 86, 487–504, 1998.

Jarvis, P. G. and McNaughton, K.: Stomatal control of transpiration: scaling up from leaf to region, Advances in ecological research, 15, 1–49, 1986.

Javaux, M., Couvreur, V., Vanderborght, J., and Vereecken, H.: Root water uptake: from three-dimensional biophysical processes to macroscopic modeling approaches, Vadose Zone Journal, 12, 2013.

Jenkinson, D., Andrew, S., Lynch, J., Goss, M., and Tinker, P.: The turnover of organic carbon and nitrogen in soil [and discussion], Philosophical Transactions of the Royal Society of London B: Biological Sciences, 329, 361–368, 1990.

Jiang, L., Yan, Y., Hararuk, O., Mikle, N., Xia, J., Shi, Z., Tjiputra, J., Wu, T., and Luo, Y.: Scale-Dependent Performance of CMIP5 Earth System Models in Simulating Terrestrial Vegetation Carbon, Journal of Climate, 28, 5217–5232, 2015.

Jung, M., Reichstein, M., Margolis, H. A., Cescatti, A., Richardson, A. D., Arain, M. A., Arneth, A., Bernhofer, C., Bonal, D., Chen, J., et al.: Global patterns of land-atmosphere fluxes of carbon dioxide, latent heat, and sensible heat derived from eddy covariance, satellite, and meteorological observations, Journal of Geophysical Research: Biogeosciences, 116, 2011.

Kaplan, J. O.: Geophysical applications of vegetation modeling, Ph.D. thesis, Lund University, 2001.

Kauppi, P. and Posch, M.: Sensitivity of boreal forests to possible climatic warming, Climatic Change, 7, 45–54, 1985.

Keeling, C. D., Bacastow, R. B., Bainbridge, A. E., Ekdahl, C. A., Guenther, P. R., Waterman, L. S., and Chin, J. F.: Atmospheric carbon dioxide variations at Mauna Loa observatory, Hawaii, Tellus, 28, 538–551, 1976.

Kelliher, F., Leuning, R., Raupach, M., and Schulze, E.-D.: Maximum conductances for evaporation from global vegetation types, Agricultural and Forest Meteorology, 73, 1–16, 1995.

Kleidon, A.: Quantifying the biologically possible range of steady-state soil and surface climates with climate model simulations, Biologia, 61, S234–S239, 2006a.

Kleidon, A.: The climate sensitivity to human appropriation of vegetation productivity and its thermodynamic characterization, Global and Planetary Change, 54, 109–127, 2006b.

Kleidon, A.: ISLSCP II Total plant-available soil water storage capacity of the rooting zone, http://daac.ornl.gov/ from Oak Ridge National Laboratory Distributed Active Archive Center, Oak Ridge, Tennessee, U.S.A., doi:10.3334/ORNLDAAC/1006, in Hall, Forrest G and Collatz, G and Meeson, B and Los, S and Brown de Colstoun, E and Landis, D (eds). ISLSCP Initiative II Collection. Data set., 2011.

Kleidon, A. and Heimann, M.: A method of determining rooting depth from a terrestrial biosphere model and its impacts on the global water and carbon cycle, Global Change Biology, 4, 275–286, 1998.

Klimarechenzentrum, D.: The ECHAM3 Atmospheric General Circulation Model, Tech. Rep. 6, Max-Planck-Institut für Meteorologie, 1993.

Knorr, W.: Annual and interannual CO_2 exchanges of the terrestrial biosphere: Process-based simulations and uncertainties, Global Ecology and Biogeography, 9, 225–252, 2000.

Knorr, W. and Schnitzler, K.-G.: Enhanced albedo feedback in North Africa from possible combined vegetation and soil-formation processes, Climate dynamics, 26, 55–63, 2006.

Köchy, M., Hiederer, R., and Freibauer, A.: Global distribution of soil organic carbon-Part 1: Masses and frequency distributions of SOC stocks for the tropics, permafrost regions, wetlands, and the world, SOIL, Volume 1, Issue 1, 2015, pp. 351-365, 1, 351–365, 2015.

Lawlor, D. and Cornic, G.: Photosynthetic carbon assimilation and associated metabolism in relation to water deficits in higher plants, Plant, Cell & Environment, 25, 275–294, 2002.

Lawson, T., Davey, P. A., Yates, S. A., Bechtold, U., Baeshen, M., Baeshen, N., Mutwakil, M. Z., Sabir, J., Baker, N. R., and Mullineaux, P. M.: C3 photosynthesis in the desert plant Rhazya stricta is fully functional at high temperatures and light intensities, New Phytologist, 201, 862–873, 2014.

Li, R. and Arora, V.: Effect of mosaic representation of vegetation in land surface schemes on simulated energy and carbon balances, Biogeosciences, 9, 593–605, 2012.

Lin, Y.-S., Medlyn, B. E., and Ellsworth, D. S.: Temperature responses of leaf net photosynthesis: the role of component processes, Tree Physiology, 32, 219–231, 2012.

Linton, M., Sperry, J. S., and Williams, D.: Limits to water transport in Juniperus osteosperma and Pinus edulis: implications for drought tolerance and regulation of transpiration, Functional Ecology, 12, 906–911, 1998.

Litton, C. M., Raich, J. W., and Ryan, M. G.: Carbon allocation in forest ecosystems, Global Change Biology, 13, 2089–2109, 2007.

Lloyd, J. and Taylor, J.: On the temperature dependence of soil respiration, Functional ecology, 8, 315–323, 1994.

Long, S.: Modification of the response of photosynthetic productivity to rising temperature by atmospheric CO2 concentrations: has its importance been underestimated?, Plant, Cell & Environment, 14, 729–739, 1991.

Loranty, M. M., Berner, L. T., Goetz, S. J., Jin, Y., and Randerson, J. T.: Vegetation controls on northern high latitude snow-albedo feedback: observations and CMIP5 model simulations, Global change biology, 20, 594–606, 2014.

Lorenz, C. and Kunstmann, H.: The hydrological cycle in three state-of-the-art reanalyses: Intercomparison and performance analysis, Journal of Hydrometeorology, 13, 1397–1420, 2012.

Louis, J., Tiedtke, M., and Geleyn, J.: A short history of the operational PBL-parameterization at ECMWF, in: Proc. Workshop on Planetary Boundary Layer Parameterization, pp. 59–79, ECMWF, Reading, United Kingdom, 1982.

Louis, J.-F.: A parametric model of vertical eddy fluxes in the atmosphere, Boundary-Layer Meteorology, 17, 187–202, 1979.

Lunkeit, F., Bottinger, M., Fraedrich, K., Jansen, H., Kirk, E., Kleidon, A., and Luksch, U.: Planet Simulator-reference manual, version 15.0, Tech. rep., Meteorologisches Institut, Universität Hamburg, 2007.

Lunkeit, F., Borth, H., Bottinger, M., Fraedrich, K., Jansen, H., Kirk, E., Kleidon, A., Luksch, U., Paiewonsky, P., S, S., Sielmann, S., and Wan, H.: Planet Simulator-reference manual, version 16, Tech. rep., Meteorologisches Institut, Universität Hamburg, 2011.

Mason, P.: The formation of areally-averaged roughness lengths, Quarterly Journal of the Royal Meteorological Society, 114, 399–420, 1988.

Maxbauer, D. P., Royer, D. L., and LePage, B. A.: High Arctic forests during the middle Eocene supported by moderate levels of atmospheric CO2, Geology, 42, 1027–1030, 2014.

McDowell, N., Pockman, W. T., Allen, C. D., Breshears, D. D., Cobb, N., Kolb, T., Plaut, J., Sperry, J., West, A., Williams, D. G., and Yepez, E. A.: Mechanisms of plant survival and mortality during drought: why do some plants survive while others succumb to drought?, New phytologist, 178, 719–739, 2008.

McGuire, A. D., Melillo, J., Joyce, L., Kicklighter, D., Grace, A., Moore, B. I., and Vorosmarty, C.: Interactions between carbon and nitrogen dynamics in estimating net primary productivity for potential vegetation in North America, Global Biogeochemical Cycles, 6, 101–124, 1992.

McLaughlin, B. C., Xu, C.-Y., Rastetter, E. B., and Griffin, K. L.: Predicting ecosystem carbon balance in a warming Arctic: the importance of long-term thermal acclimation potential and inhibitory effects of light on respiration, Global change biology, 20, 1901–1912, 2014.

Medlyn, B. E., Duursma, R. A., Eamus, D., Ellsworth, D. S., Prentice, I. C., Barton, C. V., Crous, K. Y., de Angelis, P., Freeman, M., and Wingate, L.: Reconciling the optimal and empirical approaches to modelling stomatal conductance, Global Change Biology, 17, 2134–2144, 2011.

Medlyn, B. E., Duursma, R. A., Eamus, D., Ellsworth, D. S., Colin Prentice, I., Barton, C. V., Crous, K. Y., Angelis, P., Freeman, M., and Wingate, L.: Reconciling the optimal and empirical approaches to modelling stomatal conductance, Global Change Biology, 18, 3476–3476, 2012.

Melton, J. and Arora, V.: Sub-grid scale representation of vegetation in global land surface schemes: implications for estimation of the terrestrial carbon sink, Biogeosciences, 11, 1021–1036, 2014.

Miralles, D., De Jeu, R., Gash, J., Holmes, T., and Dolman, A.: Magnitude and variability of land evaporation and its components at the global scale, Hydrology and Earth System Sciences, 15, 967–981, 2011.

Monson, R. and Baldocchi, D.: Terrestrial biosphere-atmosphere fluxes, Cambridge University Press, 2014.

Monteith, J., Huda, A., and Midya, D.: RESCAP: a resource capture model for sorghum and pearl millet, in: Modelling the growth and development of sorghum and pearl millet, edited by Virmani, S., Tandon, H., and Alagarswamy, G., vol. 12 of *Research Bulletin*, pp. 30–34, ICRISAT, Patancheru, India, 1989.

Moody, E. G., King, M. D., Schaaf, C. B., Hall, D. K., and Platnick, S.: Northern Hemisphere five-year average (2000–2004) spectral albedos of surfaces in the presence of snow: Statistics computed from Terra MODIS land products, Remote Sensing of Environment, 111, 337–345, 2007.

Mooney, H. A., Björkman, O., and Collatz, G. J.: Photosynthetic acclimation to temperature in the desert shrub, Larrea divaricata: I. Carbon dioxide exchange characteristics of intact leaves, Plant Physiology, 61, 406–410, 1978.

Mueller, B., Hirschi, M., Jimenez, C., Ciais, P., Dirmeyer, P., Dolman, A., Fisher, J., Jung, M., Ludwig, F., Maignan, F., et al.: Benchmark products for land evapotranspiration: LandFlux-EVAL multi-data set synthesis, Hydrology and Earth System Sciences, 17, 3707–3720, 2013.

NASA LP DAAC: MODIS Terra+Aqua BRDF/Albedo Snow-free Quality 16-Day L3 Global 0.05Deg CMG V005 (MCD43C2), https://lpdaac.usgs.gov from NASA EOSDIS Land Processes DAAC, USGS Earth Resources Observation and Science (EROS) Center, Sioux Falls, South Dakota, accessed: 2016-02, 2008a.

NASA LP DAAC: MODIS Terra+Aqua BRDF/Albedo 16-Day L3 Global 0.05Deg CMG V005 (MCD43C3), https://lpdaac.usgs.gov from NASA EOSDIS Land Processes DAAC, USGS Earth Resources Observation and Science (EROS) Center, Sioux Falls, South Dakota, accessed: 2014-12, 2008b.

Nilson, T.: A theoretical analysis of the frequency of gaps in plant stands, Agricultural Meteorology, 8, 25–38, 1971.

Oke, T.: Boundary layer climates, Methuen, London, 2nd edn. edn., 1987.

Olson, D. M., Dinerstein, E., Wikramanayake, E. D., Burgess, N. D., Powell, G. V., Underwood, E. C., D'amico, J. A., Itoua, I., Strand, H. E., Morrison, J. C., et al.: Terrestrial Ecoregions of the World: A New Map of Life on Earth A new global map of terrestrial ecoregions provides an innovative tool for conserving biodiversity, BioScience, 51, 933–938, 2001.

Olson, J., Watts, J., and Allison, L.: Major world ecosystem complexes ranked by carbon in live vegetation: A Database (NDP-017)., http://cdiac.ornl.gov/epubs/ndp/ndp017/ndp017_1985.html from Carbon Dioxide Information Center, Oak Ridge National Laboratory, Oak Ridge, Tennessee, U.S.A., doi:10.3334/CDIAC/lue.ndp017, accessed: 2016-03; revised in 2001, 1985.

Pavlick, R., Drewry, D. T., Bohn, K., Reu, B., and Kleidon, A.: The Jena Diversity-Dynamic Global Vegetation Model (JeDi-DGVM): a diverse approach to representing terrestrial biogeography and biogeochemistry based on plant functional trade-offs, Biogeosciences, 10, 4137–4177, 2013.

Piao, S., Sitch, S., Ciais, P., Friedlingstein, P., Peylin, P., Wang, X., Ahlström, A., Anav, A., Canadell, J. G., Cong, N., et al.: Evaluation of terrestrial carbon cycle models for their response to climate variability and to CO2 trends, Global Change Biology, 19, 2117–2132, 2013.

Pisek, J., Chen, J. M., Lacaze, R., Sonnentag, O., and Alikas, K.: Expanding global mapping of the foliage clumping index with multi-angular POLDER three measurements: Evaluation and topographic compensation, ISPRS Journal of Photogrammetry and Remote Sensing, 65, 341–346, 2010.

Pisek, J., Sonnentag, O., Richardson, A. D., and Mõttus, M.: Is the spherical leaf inclination angle distribution a valid assumption for temperate and boreal broadleaf tree species?, Agricultural and Forest Meteorology, 169, 186–194, 2013.

Prentice, I. C., Cramer, W., Harrison, S. P., Leemans, R., Monserud, R. A., and Solomon, A. M.: Special paper: a global biome model based on plant physiology and dominance, soil properties and climate, Journal of biogeography, 19, 117–134, 1992.

Prentice, I. C., Dong, N., Gleason, S. M., Maire, V., and Wright, I. J.: Balancing the costs of carbon gain and water transport: testing a new theoretical framework for plant functional ecology, Ecology letters, 17, 82–91, 2014.

Ramankutty, N. and Foley, J. A.: Estimating historical changes in global land cover: Croplands from 1700 to 1992, Global biogeochemical cycles, 13, 997–1027, 1999.

Raupach, M.: Influences of local feedbacks on land–air exchanges of energy and carbon, Global Change Biology, 4, 477–494, 1998.

Raupach, M. and Finnigan, J.: Single layer models of evaporation from plant canopies are incorrect but useful, whereas multilayer models are correct but useless: discuss, Australian journal of plant physiology, 15, 705–716, 1988.

Rechid, D., Raddatz, T. J., and Jacob, D.: Parameterization of snow-free land surface albedo as a function of vegetation phenology based on MODIS data and applied in climate modelling, Theoretical and Applied Climatology, 95, 245–255, 2009.

Roeckner, E., Bäuml, G., Bonaventura, L., Brokopf, R., Esch, M., Giorgetta, M., Hagemann, S., Kirchner, I., Kornblueh, L., Manzini, E., et al.: The atmospheric general circulation model ECHAM 5. PART I: Model description, Tech. Rep. 349, Max-Planck-Institut für Meteorologie, 2003.

Roesch, A. and Roeckner, E.: Assessment of snow cover and surface albedo in the ECHAM5 general circulation model, Journal of Climate, 19, 3828–3843, 2006.

Roesch, A., Wild, M., Gilgen, H., and Ohmura, A.: A new snow cover fraction parametrization for the ECHAM4 GCM, Climate Dynamics, 17, 933–946, 2001.

Sage, R. F. and Kubien, D. S.: The temperature response of C3 and C4 photosynthesis, Plant, Cell & Environment, 30, 1086–1106, 2007.

Schaefer, K., Schwalm, C. R., Williams, C., Arain, M. A., Barr, A., Chen, J. M., Davis, K. J., Dimitrov, D., Hilton, T. W., Hollinger, D. Y., et al.: A model-data comparison of gross primary productivity: Results from the North American Carbon Program site synthesis, Journal of Geophysical Research: Biogeosciences, 117, 2012.

Schlesinger, W. H. and Jasechko, S.: Transpiration in the global water cycle, Agricultural and Forest Meteorology, 189, 115–117, 2014.

Sellers, P. J., Tucker, C. J., Collatz, G. J., Los, S. O., Justice, C. O., Dazlich, D. A., and Randall, D. A.: A revised land surface parameterization (SiB2) for atmospheric GCMs. Part II: The generation of global fields of terrestrial biophysical parameters from satellite data, Journal of climate, 9, 706–737, 1996.

Serbin, S. P., Ahl, D. E., and Gower, S. T.: Spatial and temporal validation of the MODIS LAI and FPAR products across a boreal forest wildfire chronosequence, Remote Sensing of Environment, 133, 71–84, 2013.

Shinozaki, K., Yoda, K., Hozumi, K., and Kira, T.: A quantitative analysis of plant form-the pipe model theory: I. Basic analyses, Japanese Journal of Ecology, 14, 97–105, 1964.

Shuttleworth, W. J.: Evaporation from Amazonian rainforest, Proceedings of the Royal Society of London B: Biological Sciences, 233, 321–346, 1988.

Sitch, S., Smith, B., Prentice, I. C., Arneth, A., Bondeau, A., Cramer, W., Kaplan, J., Levis, S., Lucht, W., Sykes, M., Thonicke, K., and Venevsky, S.: Evaluation of ecosystem dynamics, plant geography and terrestrial carbon cycling in the LPJ dynamic global vegetation model, Global Change Biology, 9, 161–185, 2003.

Sitch, S., Huntingford, C., Gedney, N., Levy, P., Lomas, M., Piao, S., Betts, R., Ciais, P., Cox, P., Friedlingstein, P., Jones, C., Prentice, I., and Woodward, F.: Evaluation of the terrestrial carbon cycle, future plant geography and climate-carbon cycle feedbacks using five Dynamic Global Vegetation Models (DGVMs), Global Change Biology, 14, 2015–2039, 2008.

Sperry, J., Hacke, U., Oren, R., and Comstock, J.: Water deficits and hydraulic limits to leaf water supply, Plant, Cell & Environment, 25, 251–263, 2002.

Tian, H., Lu, C., Yang, J., Banger, K., Huntzinger, D. N., Schwalm, C. R., Michalak, A. M., Cook, R., Ciais, P., Hayes, D., et al.: Global patterns and controls of soil organic carbon dynamics as simulated by multiple terrestrial biosphere models: Current status and future directions, Global Biogeochemical Cycles, 29, 775–792, 2015.

Todd-Brown, K., Randerson, J., Post, W., Hoffman, F., Tarnocai, C., Schuur, E., and Allison, S.: Causes of variation in soil carbon simulations from CMIP5 Earth system models and comparison with observations, Biogeosciences, 10, 1717–1736, 2013.

Tyree, M. T. and Sperry, J. S.: Do woody plants operate near the point of catastrophic xylem dysfunction caused by dynamic water stress? Answers from a model, Plant physiology, 88, 574–580, 1988.

Vamborg, F., Brovkin, V., and Claussen, M.: The effect of a dynamic background albedo scheme on Sahel/Sahara precipitation during the mid-Holocene, Climate of the Past, 7, 117–131, 2011.

Vamborg, F., Brovkin, V., and Claussen, M.: Background albedo dynamics improve simulated precipitation variability in the Sahel region, Earth System Dynamics, 5, 89–101, 2014.

van de Griend, A. A. and Owe, M.: Bare soil surface resistance to evaporation by vapor diffusion under semiarid conditions, Water Resources Research, 30, 181–188, 1994.

Van Oijen, M., Schapendonk, A., and Höglind, M.: On the relative magnitudes of photosynthesis, respiration, growth and carbon storage in vegetation, Annals of Botany, 105, 739–797, 2010.

Wang-Erlandsson, L., van der Ent, R., Gordon, L., and Savenije, H.: Contrasting roles of interception and transpiration in the hydrological cycle–Part 1: Temporal characteristics over land, Earth System Dynamics, 5, 441–469, 2014.

Way, D. A. and Yamori, W.: Thermal acclimation of photosynthesis: on the importance of adjusting our definitions and accounting for thermal acclimation of respiration, Photosynthesis research, 119, 89–100, 2014.

Wieder, W., Boehnert, J., Bonan, G., and Langseth, M.: Regridded Harmonized World Soil Database v1.2. Data set, http://daac.ornl.gov/ from Oak Ridge National Laboratory Distributed Active Archive Center, Oak Ridge, Tennessee, U.S.A., doi:10.3334/ORNLDAAC/1247, accessed: 2016-02, 2011.

Williamson, M., Lenton, T., Shepherd, J., and Edwards, N.: An efficient numerical terrestrial scheme (ENTS) for Earth system modelling, Ecological Modelling, 198, 362–374, 2006.

Wu, J., Albert, L. P., Lopes, A. P., Restrepo-Coupe, N., Hayek, M., Wiedemann, K. T., Guan, K., Stark, S. C., Christoffersen, B., Prohaska, N., et al.: Leaf development and demography explain photosynthetic seasonality in Amazon evergreen forests, Science, 351, 972–976, 2016.

Yamori, W., Hikosaka, K., and Way, D. A.: Temperature response of photosynthesis in C3, C4, and CAM plants: temperature acclimation and temperature adaptation, Photosynthesis research, 119, 101–117, 2014.

Yuan, H., Dai, Y., Xiao, Z., Ji, D., and Shangguan, W.: Reprocessing the MODIS Leaf Area Index products for land surface and climate modelling, Remote Sensing of Environment, 115, 1171–1187, 2011.

Yuan, W., Liu, S., Zhou, G., Zhou, G., Tieszen, L. L., Baldocchi, D., Bernhofer, C., Gholz, H., Goldstein, A. H., Goulden, M. L., et al.: Deriving a light use efficiency model from eddy covariance flux data for predicting daily gross primary production across biomes, Agricultural and Forest Meteorology, 143, 189–207, 2007.

Zhang, X., Liang, S., Wang, G., Yao, Y., Jiang, B., and Cheng, J.: Evaluation of the Reanalysis Surface Incident Shortwave Radiation Products from NCEP, ECMWF, GSFC, and JMA Using Satellite and Surface Observations., Remote Sensing, 8, 2016.

Geosci. Model Dev. Discuss., doi:10.5194/gmd-2017-75, 2017
Manuscript under review for journal Geosci. Model Dev.
Discussion started: 5 May 2017

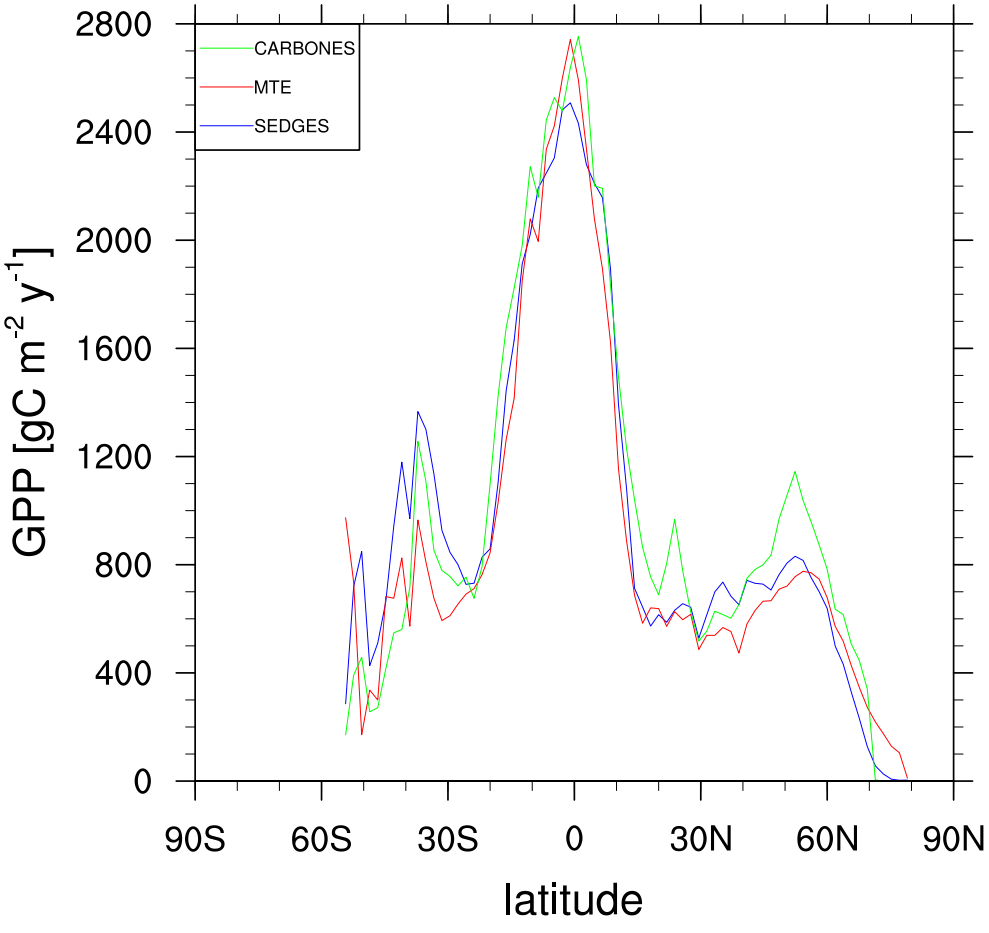

Figure 1. Zonal annual mean climatology of gross primary productivity (GPP) for SEDGES and the two reference datasets, MTE and CARBONES, for 1990-2009 over non-glaciated land.

Geosci. Model Dev. Discuss., doi:10.5194/gmd-2017-75, 2017
Manuscript under review for journal Geosci. Model Dev.
Discussion started: 5 May 2017

Geoscientific Model Development Discussions
Open Access
EGU

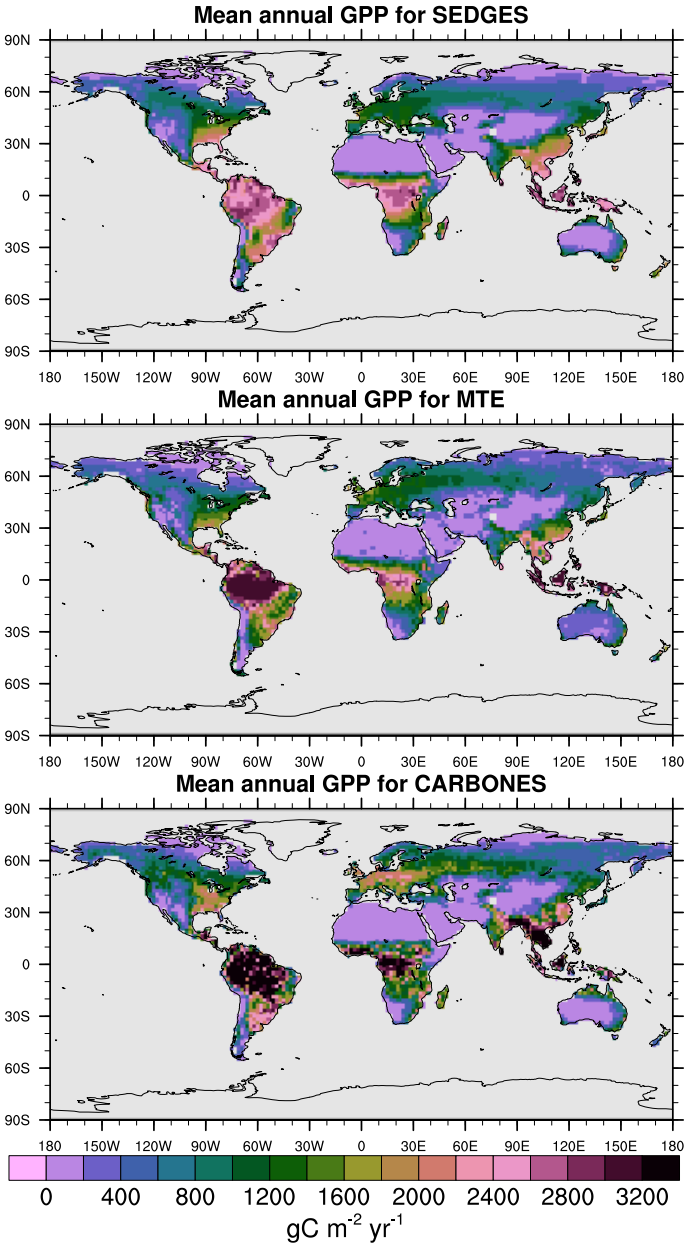

Figure 2. Annual mean climatology of gross primary productivity (GPP) for SEDGES and the two reference datasets, MTE and CARBONES, for 1990-2009 over non-glaciated land.

Geosci. Model Dev. Discuss., doi:10.5194/gmd-2017-75, 2017
Manuscript under review for journal Geosci. Model Dev.
Discussion started: 5 May 2017

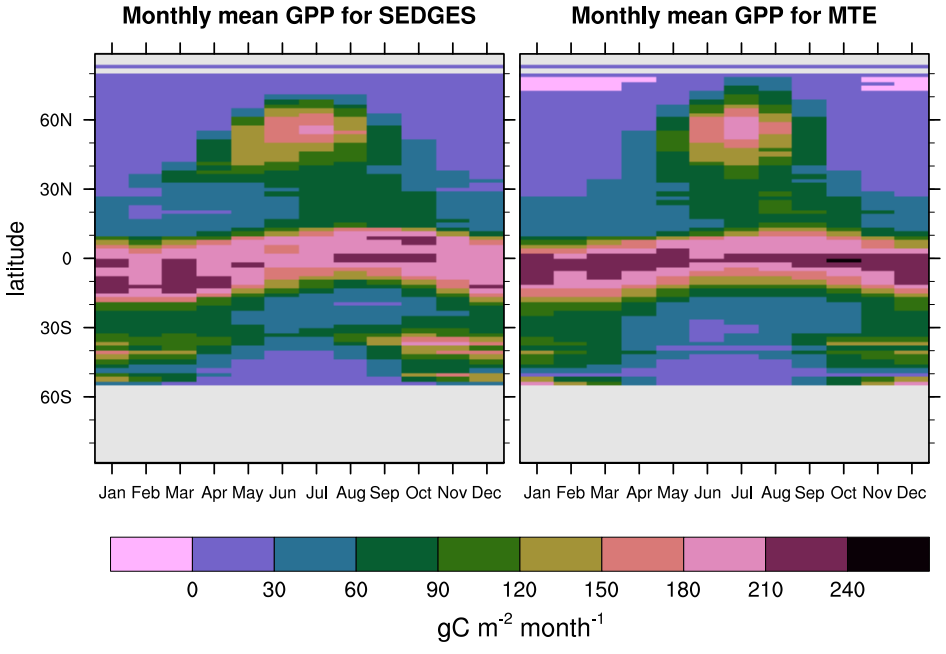

Figure 3. Zonal monthly mean climatology of gross primary productivity (GPP) for SEDGES and the MTE reference dataset for 1982-2010 over non-glaciated land.

Geosci. Model Dev. Discuss., doi:10.5194/gmd-2017-75, 2017
Manuscript under review for journal Geosci. Model Dev.
Discussion started: 5 May 2017

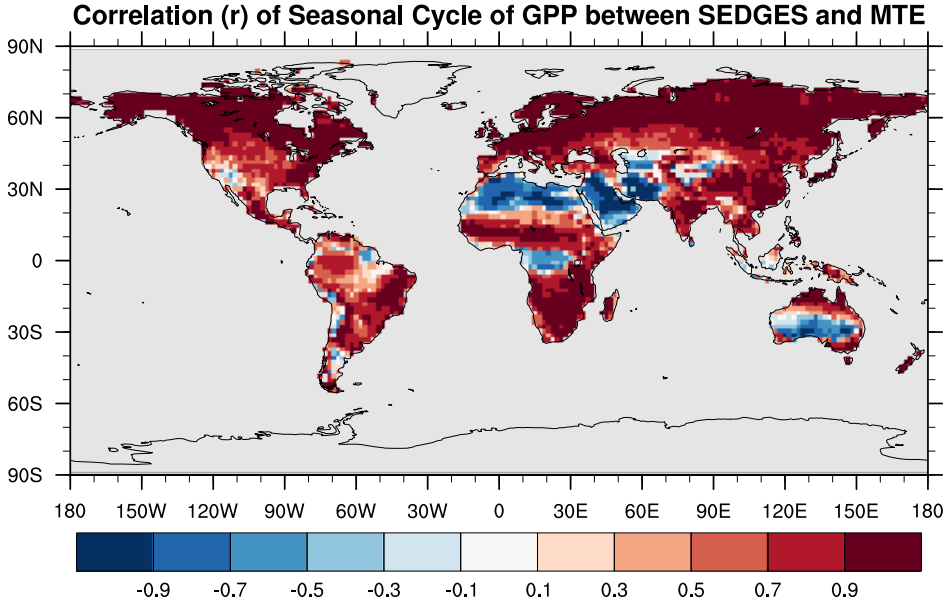

Figure 4. Pearson correlation coefficients of the seasonal cycle (i.e. of the climatological monthly means) between SEDGES and the MTE reference dataset for the 1986-2005 period.

Geosci. Model Dev. Discuss., doi:10.5194/gmd-2017-75, 2017
Manuscript under review for journal Geosci. Model Dev.
Discussion started: 5 May 2017

Geoscientific Model Development Discussions

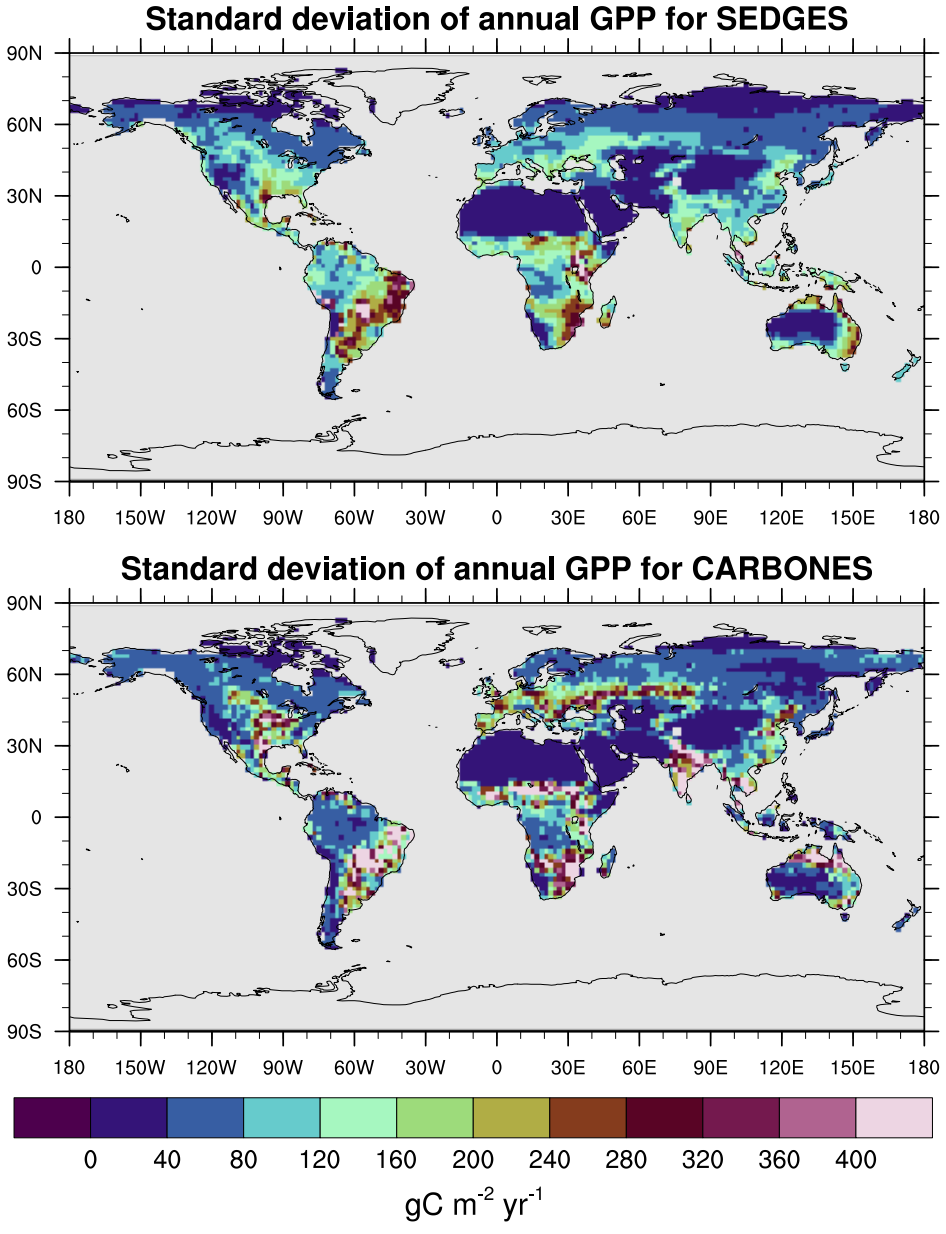

Figure 5. Interannual variability of GPP for SEDGES and the CARBONES reference dataset for the 1990-2009 period.

Geosci. Model Dev. Discuss., doi:10.5194/gmd-2017-75, 2017
Manuscript under review for journal Geosci. Model Dev.
Discussion started: 5 May 2017

Geoscientific Model Development Discussions

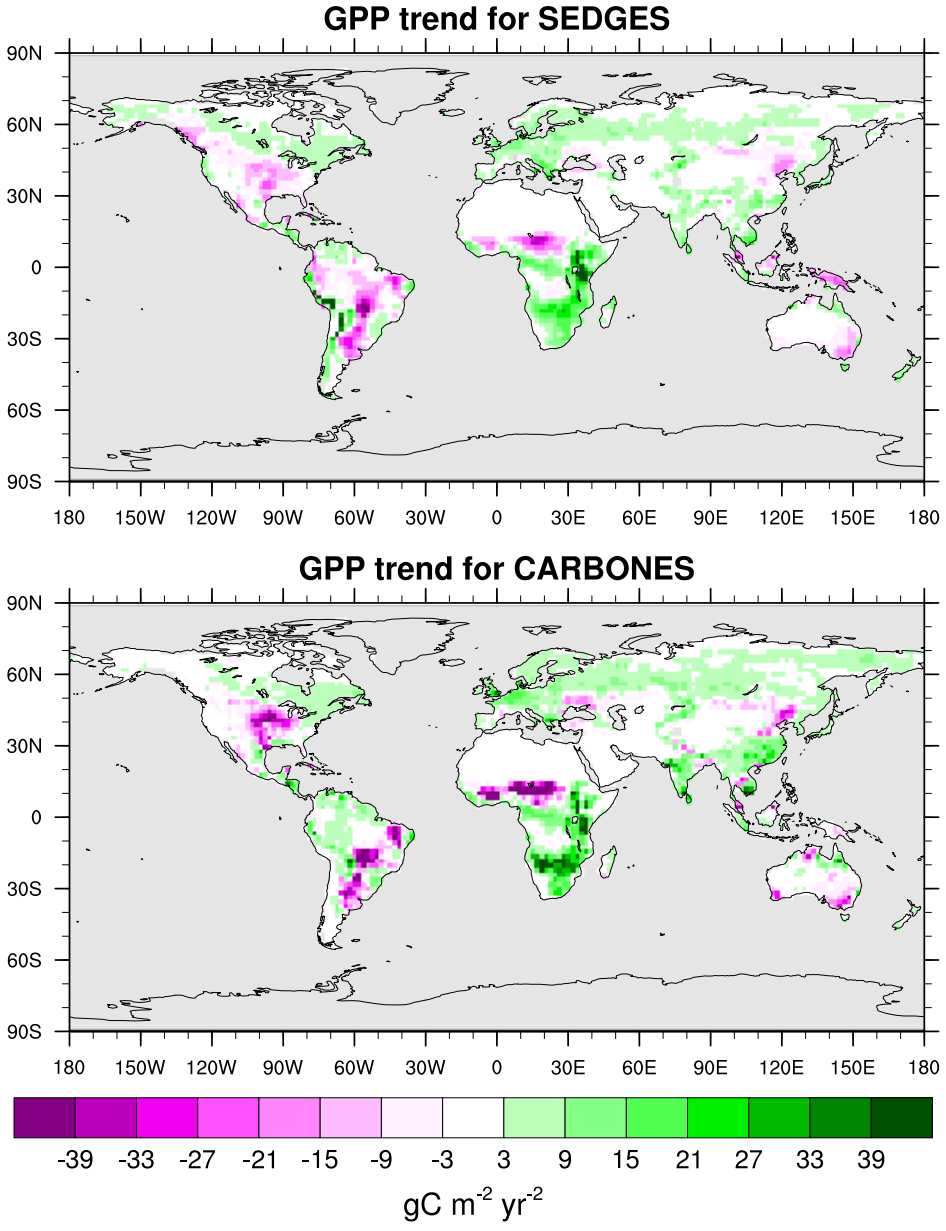

Figure 6. Linear regression trend in annual GPP for SEDGES and the CARBONES reference dataset for 1990-2009.

Geosci. Model Dev. Discuss., doi:10.5194/gmd-2017-75, 2017
Manuscript under review for journal Geosci. Model Dev.
Discussion started: 5 May 2017

Geoscientific Model Development Discussions

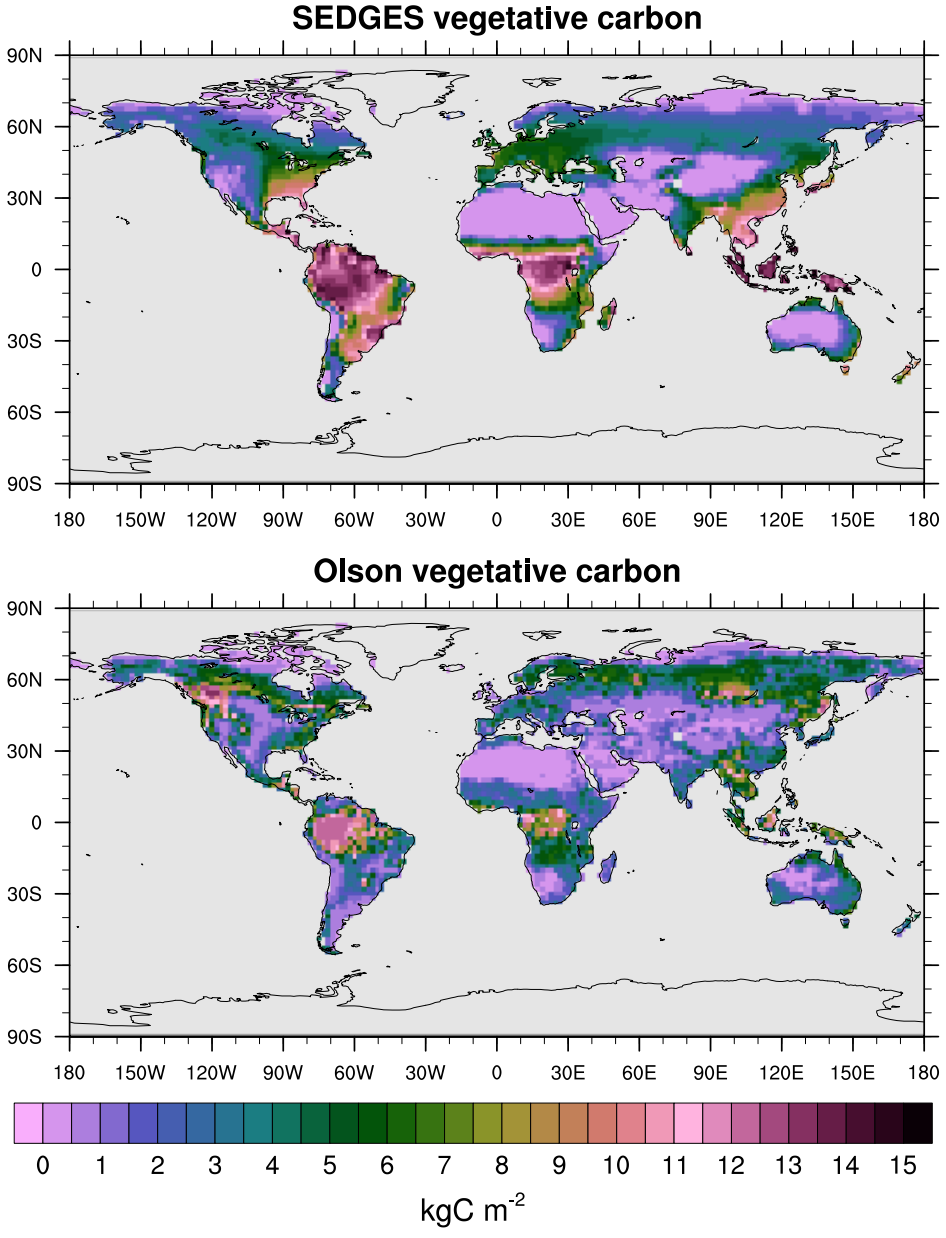

Figure 7. Vegetative carbon for SEDGES: mean over 1981-2010 in the transient CO_2 simulation; vegetative carbon from the Olson et al. (1985) reference dataset, which represents pre-Iron Age vegetation save for the most extreme anthropgenic land cover changes.

Geosci. Model Dev. Discuss., doi:10.5194/gmd-2017-75, 2017
Manuscript under review for journal Geosci. Model Dev.
Discussion started: 5 May 2017

Geoscientific Model Development Discussions

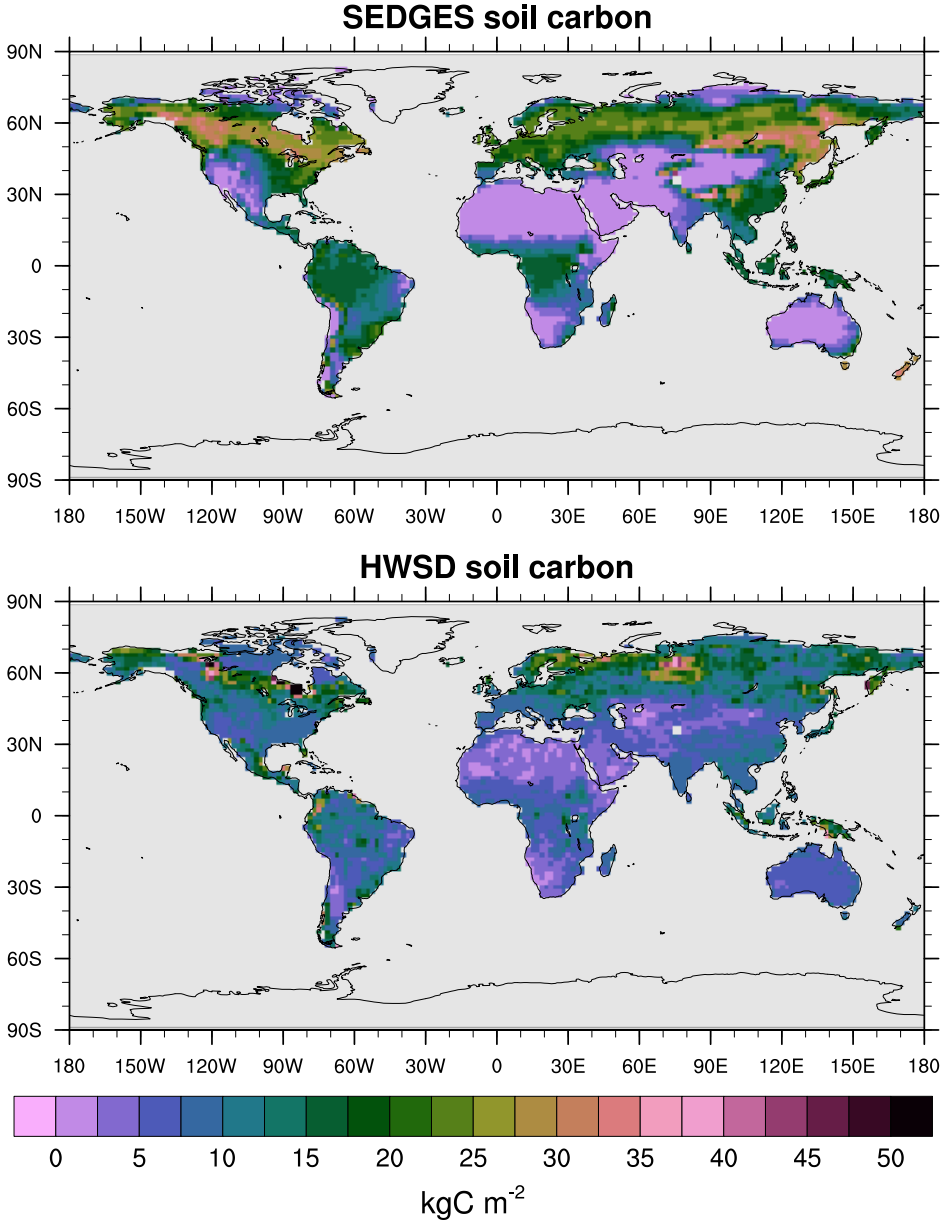

Figure 8. Soil carbon for SEDGES: mean over 1981-2010 of the transient CO_2 simulation; Soil carbon from the Harmonized World Soil Database (HWSD) reference dataset (Wieder et al., 2011). The HWSD dataset has values for the top meter of the profile, only.

Geosci. Model Dev. Discuss., doi:10.5194/gmd-2017-75, 2017
Manuscript under review for journal Geosci. Model Dev.
Discussion started: 5 May 2017

Geoscientific Model Development Discussions

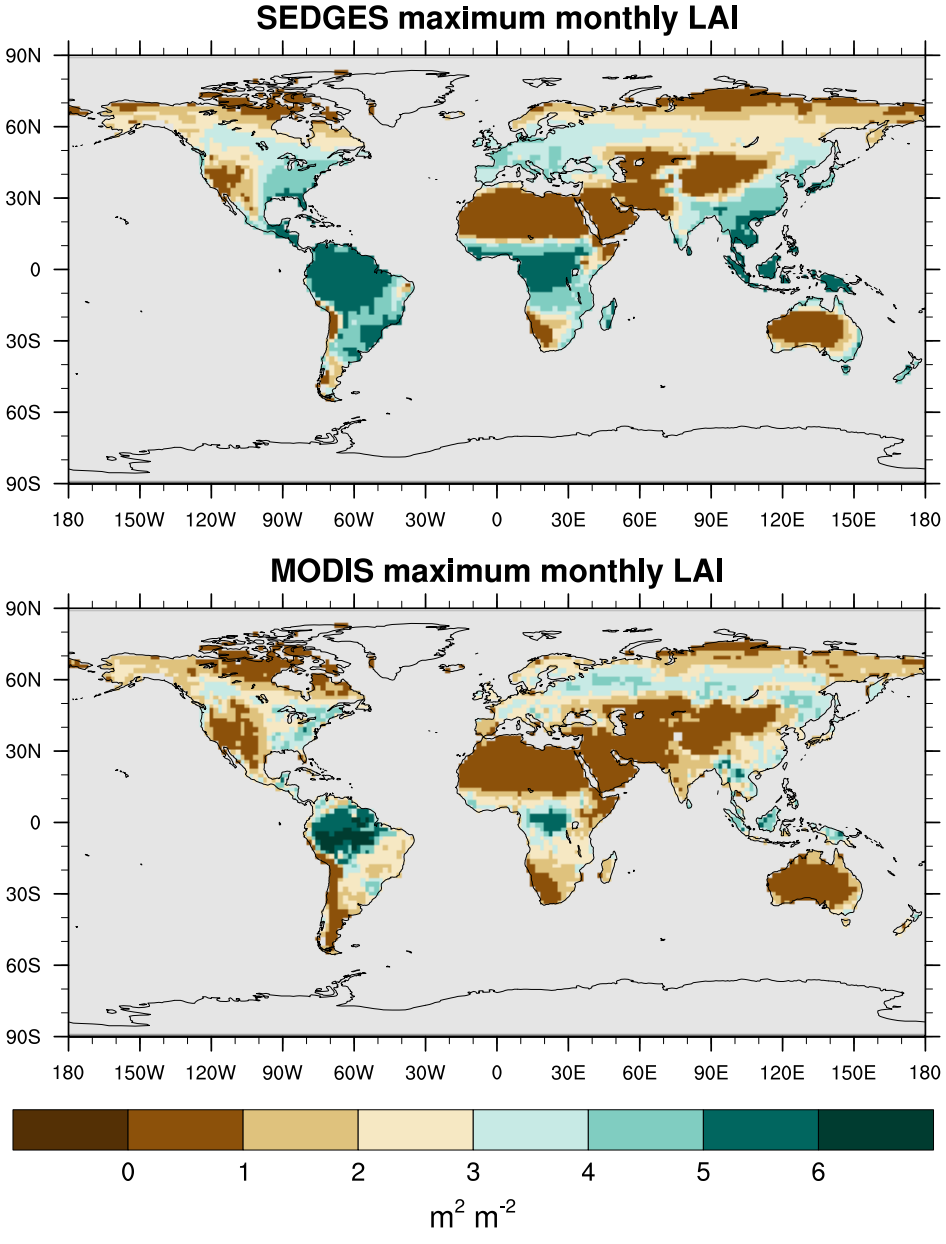

Figure 9. Maximum leaf area index (LAI) of the monthly mean climatology for SEDGES and for the BNU MODIS-based reference dataset for the 2001-2010 period.

Geosci. Model Dev. Discuss., doi:10.5194/gmd-2017-75, 2017
Manuscript under review for journal Geosci. Model Dev.
Discussion started: 5 May 2017

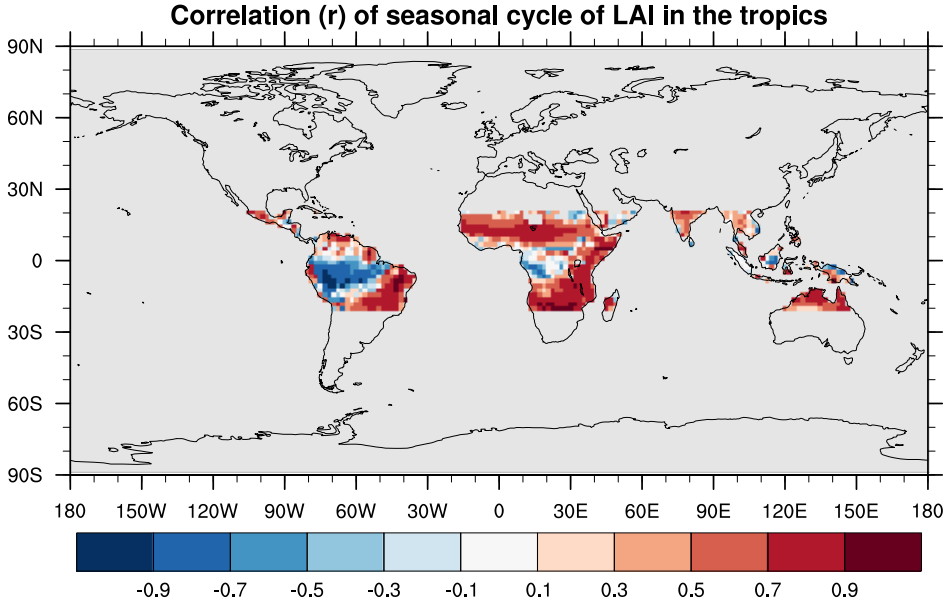

Figure 10. Temporal correlation at each grid point in the tropics (-20° to 20°) between the monthly mean climatologies of LAI for 2001-2010 of SEDGES and of the BNU MODIS-based reference dataset. Some desert grid points do not have values because they have LAI's of 0 in one or both sets of data for all 12 months.

Geosci. Model Dev. Discuss., doi:10.5194/gmd-2017-75, 2017
Manuscript under review for journal Geosci. Model Dev.
Discussion started: 5 May 2017

Geoscientific Model Development Discussions
Open Access
EGU

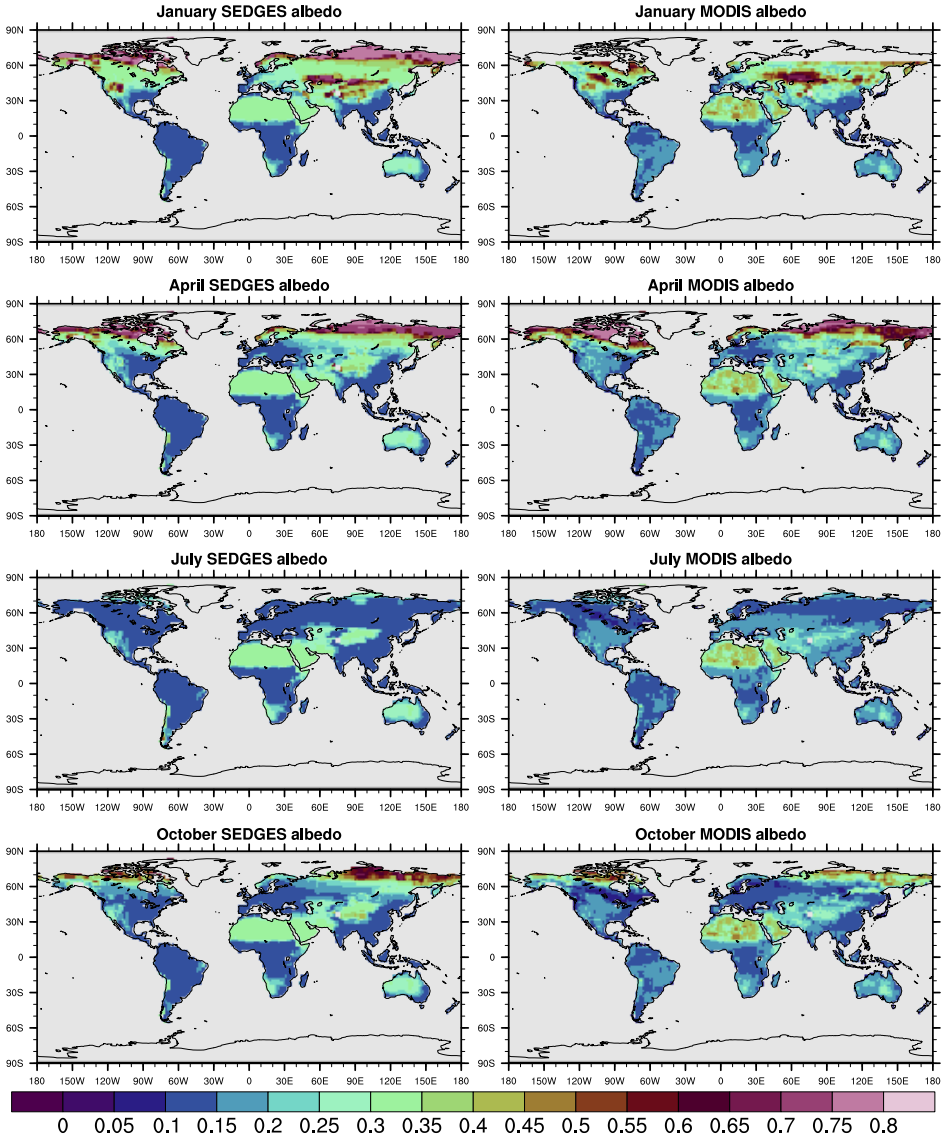

Figure 11. Left: SEDGES monthly mean climatologies of surface albedo for 2001-2010. Right: MODIS monthly mean climatologies of white sky albedo for 2001-2010 (NASA LP DAAC, b).

Geosci. Model Dev. Discuss., doi:10.5194/gmd-2017-75, 2017
Manuscript under review for journal Geosci. Model Dev.
Discussion started: 5 May 2017

Geoscientific Model Development Discussions
Open Access
EGU

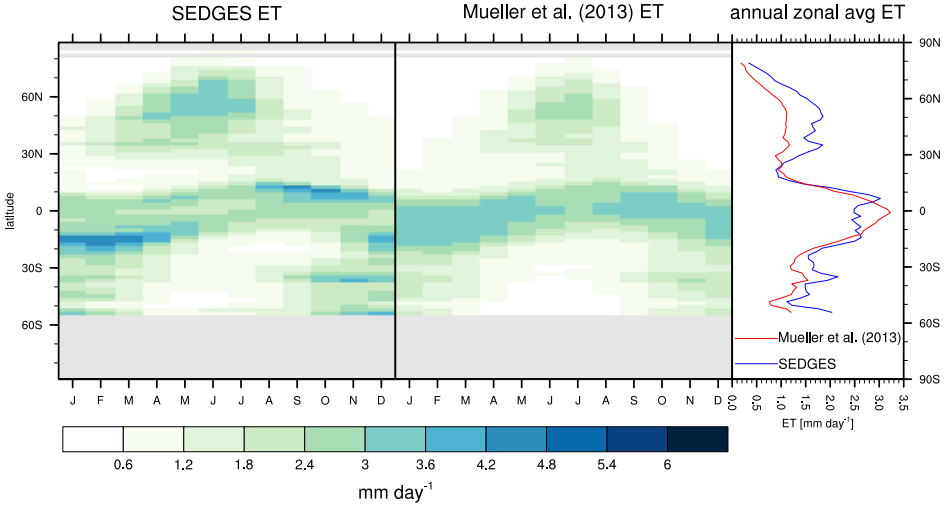

Figure 12. Zonal monthly mean and zonal annual mean climatologies of evapotranspiration (ET) for SEDGES and the Mueller et al. (2013) reference dataset for the 1989-2005 period over non-glaciated land.

Geosci. Model Dev. Discuss., doi:10.5194/gmd-2017-75, 2017
Manuscript under review for journal Geosci. Model Dev.
Discussion started: 5 May 2017

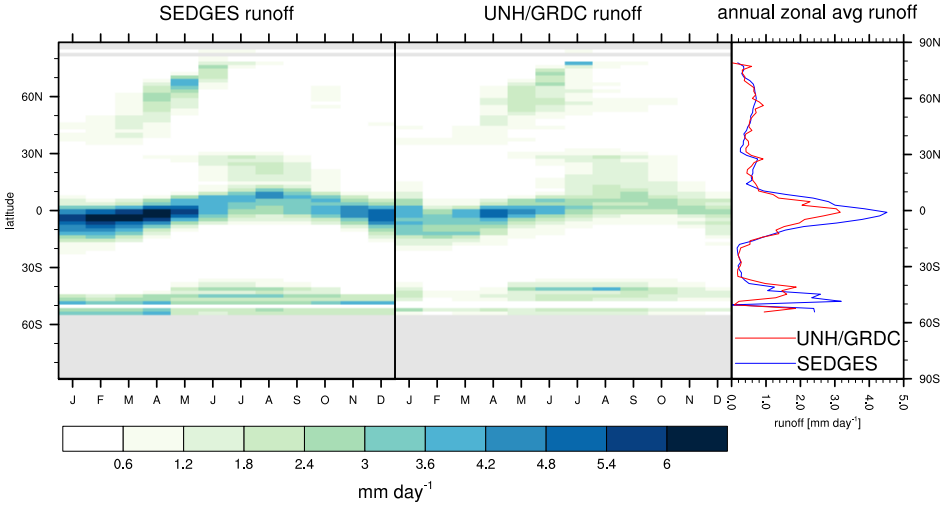

Figure 13. Zonal monthly mean and zonal annual mean climatologies of runoff for SEDGES and the UNH-GRDC reference dataset (Fekete et al., 2002) over non-glaciated land.

Geosci. Model Dev. Discuss., doi:10.5194/gmd-2017-75, 2017
Manuscript under review for journal Geosci. Model Dev.
Discussion started: 5 May 2017

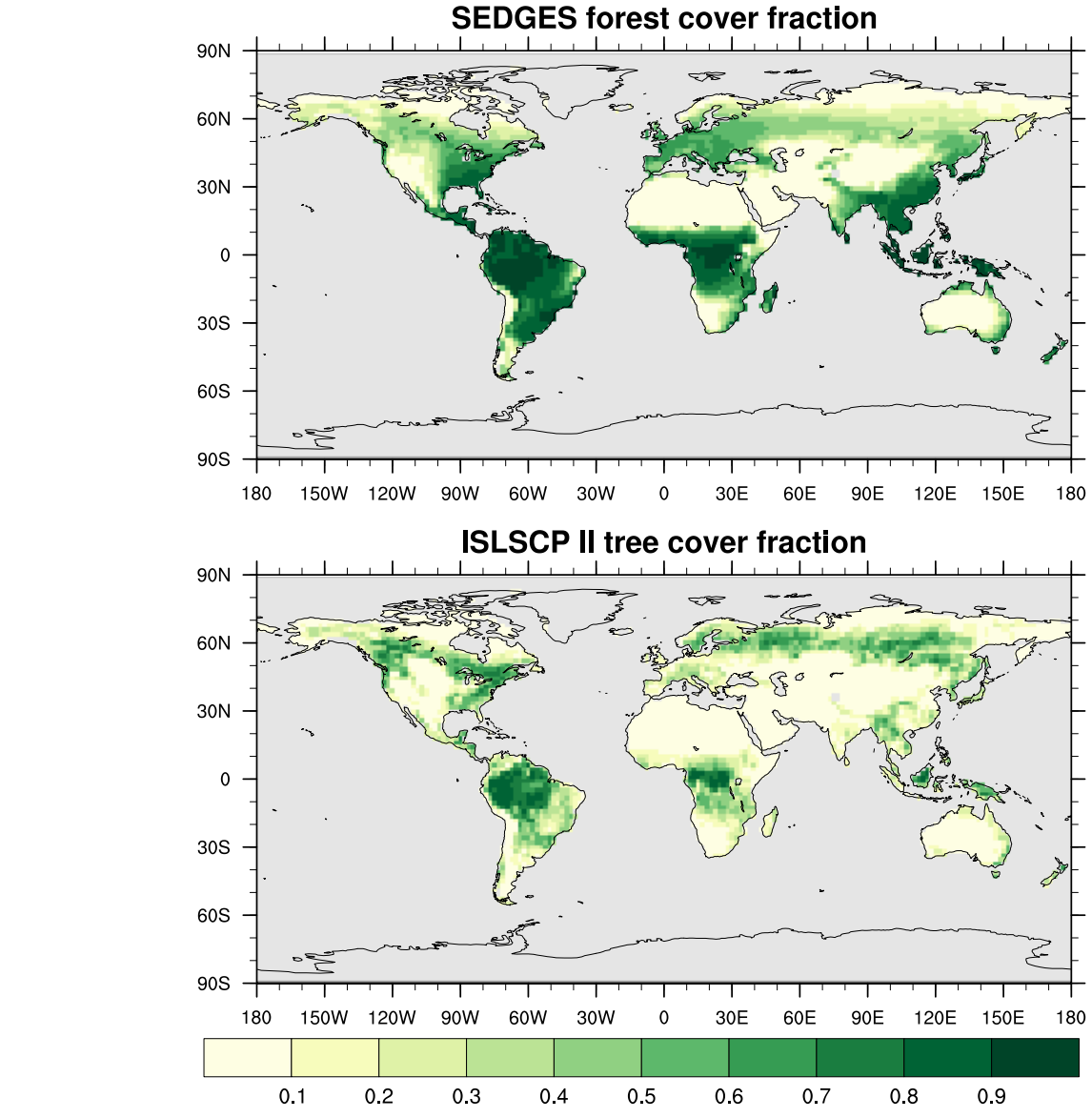

Figure 14. Mean forest cover fraction for SEDGES and tree cover fraction from the reference ISLSCP II dataset (DeFries and Hansen, 2009).

Geosci. Model Dev. Discuss., doi:10.5194/gmd-2017-75, 2017
Manuscript under review for journal Geosci. Model Dev.
Discussion started: 5 May 2017

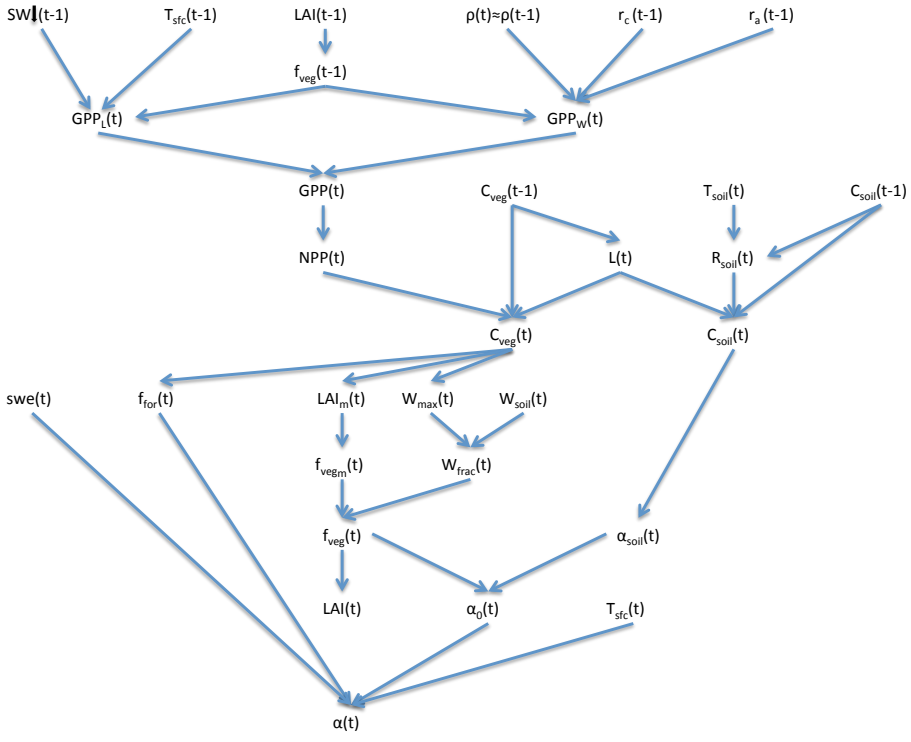

Figure 15. Variable dependencies and updating in SEDGES

Geosci. Model Dev. Discuss., doi:10.5194/gmd-2017-75, 2017
Manuscript under review for journal Geosci. Model Dev.
Discussion started: 5 May 2017

Geoscientific Model Development Discussions

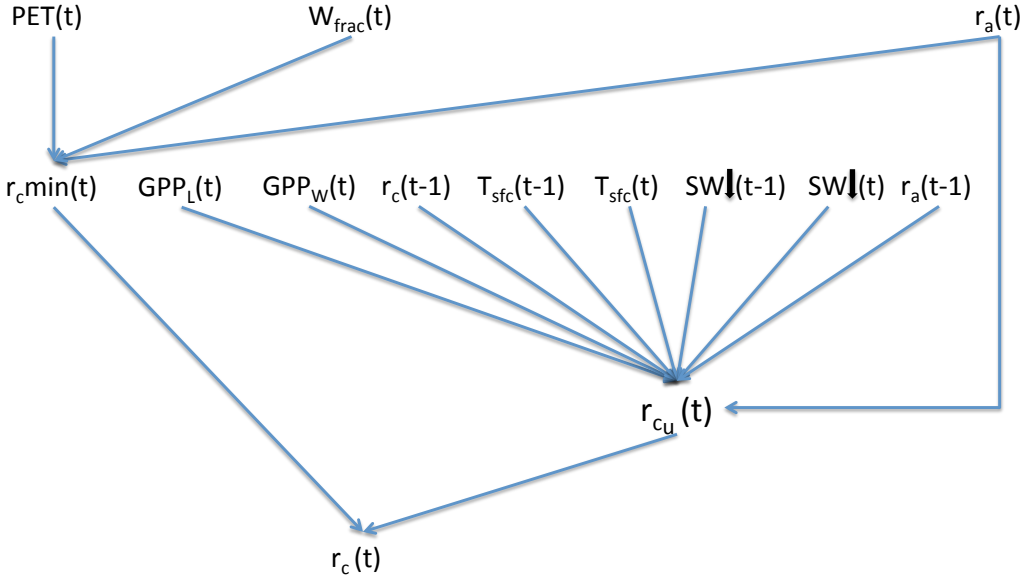

Figure 16. Canopy resistance dependencies and updating in SEDGES